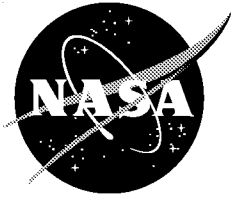


NASA/TM-1999-206586



Estimated Benefits of Variable-Geometry Wing Camber Control for Transport Aircraft

*Alexander Bolonkin
Senior Research Associate of the National Research Council
Dryden Flight Research Center
Edwards, California*

*Glenn B. Gilyard
Dryden Flight Research Center
Edwards, California*

October 1999

The NASA STI Program Office . . . in Profile

Since its founding, NASA has been dedicated to the advancement of aeronautics and space science. The NASA Scientific and Technical Information (STI) Program Office plays a key part in helping NASA maintain this important role.

The NASA STI Program Office is operated by Langley Research Center, the lead center for NASA's scientific and technical information. The NASA STI Program Office provides access to the NASA STI Database, the largest collection of aeronautical and space science STI in the world. The Program Office is also NASA's institutional mechanism for disseminating the results of its research and development activities. These results are published by NASA in the NASA STI Report Series, which includes the following report types:

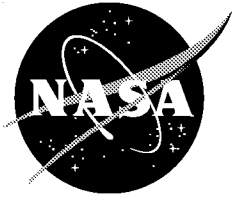
- **TECHNICAL PUBLICATION.** Reports of completed research or a major significant phase of research that present the results of NASA programs and include extensive data or theoretical analysis. Includes compilations of significant scientific and technical data and information deemed to be of continuing reference value. NASA's counterpart of peer-reviewed formal professional papers but has less stringent limitations on manuscript length and extent of graphic presentations.
- **TECHNICAL MEMORANDUM.** Scientific and technical findings that are preliminary or of specialized interest, e.g., quick release reports, working papers, and bibliographies that contain minimal annotation. Does not contain extensive analysis.
- **CONTRACTOR REPORT.** Scientific and technical findings by NASA-sponsored contractors and grantees.
- **CONFERENCE PUBLICATION.** Collected papers from scientific and technical conferences, symposia, seminars, or other meetings sponsored or cosponsored by NASA.
- **SPECIAL PUBLICATION.** Scientific, technical, or historical information from NASA programs, projects, and mission, often concerned with subjects having substantial public interest.
- **TECHNICAL TRANSLATION.** English-language translations of foreign scientific and technical material pertinent to NASA's mission.

Specialized services that complement the STI Program Office's diverse offerings include creating custom thesauri, building customized databases, organizing and publishing research results . . . even providing videos.

For more information about the NASA STI Program Office, see the following:

- Access the NASA STI Program Home Page at <http://www.sti.nasa.gov>
- E-mail your question via the Internet to help@sti.nasa.gov
- Fax your question to the NASA Access Help Desk at (301) 621-0134
- Telephone the NASA Access Help Desk at (301) 621-0390
- Write to:
NASA Access Help Desk
NASA Center for AeroSpace Information
7121 Standard Drive
Hanover, MD 21076-1320

NASA/TM-1999-206586



Estimated Benefits of Variable-Geometry Wing Camber Control for Transport Aircraft

Alexander Bolonkin
Senior Research Associate of the National Research Council
Dryden Flight Research Center
Edwards, California

Glenn B. Gilyard
Dryden Flight Research Center
Edwards, California

National Aeronautics and
Space Administration

Dryden Flight Research Center
Edwards, California 93523-0273

October 1999

NOTICE

Use of trade names or names of manufacturers in this document does not constitute an official endorsement of such products or manufacturers, either expressed or implied, by the National Aeronautics and Space Administration.

Available from the following:

NASA Center for AeroSpace Information (CASI)
7121 Standard Drive
Hanover, MD 21076-1320
(301) 621-0390

National Technical Information Service (NTIS)
5285 Port Royal Road
Springfield, VA 22161-2171
(703) 487-4650

CONTENTS

| | <u>Page</u> |
|---|-------------|
| ABSTRACT | 1 |
| NOMENCLATURE | 1 |
| Symbols | 1 |
| Subscripts | 3 |
| INTRODUCTION | 3 |
| WING CAMBER CONTROL BACKGROUND..... | 4 |
| ANALYTICAL DEVELOPMENT OF VARIABLE-GEOMETRY | |
| WING CAMBER OPTIMIZATION | 5 |
| Development of Low-Speed Lift and Drag Coefficient Expressions as a Function of Camber..... | 5 |
| Influence of Shape on Aerodynamics..... | 6 |
| Influence of Mach Number on Aerodynamics | 7 |
| Influence of Pitching Moments on Aerodynamics | 8 |
| General Correction for Nonparabolic Polar | 9 |
| Summary of Equations | 9 |
| Influence of the Lift-to-Drag Ratio on Fuel Consumption | 10 |
| CALCULATION OF VARIABLE-CAMBER BENEFITS FOR A TYPICAL WIDE-BODY TRANSPORT..... | 11 |
| Database Development | 11 |
| C_D | 12 |
| $\Delta C_{D_{\min}}(\delta)$ | 12 |
| $\Delta C_{D_{np}}$ | 12 |
| C_{D_i} | 13 |
| $\Delta C_{D_{\text{wave}}}$ | 13 |
| ΔC_{D_m} | 13 |
| ΔC_{D^c} | 14 |
| Calculation of Variable-Camber Benefit from Database | 14 |
| ESTIMATED BENEFITS OF VARIABLE CAMBER FOR THE L-1011 EXAMPLE | 14 |
| Low-Speed Flight (Mach 0.60) | 14 |
| Cruise Flight (Mach 0.83)..... | 15 |
| Application of Variable Camber | 15 |
| CONCLUDING REMARKS | 16 |
| REFERENCES | 18 |

FIGURES

| | <u>Page</u> |
|---|-------------|
| 1. Lift coefficient plotted as a function of angle of attack (schematic)..... | 20 |
| 2. Drag coefficient plotted as a function of angle of attack (schematic)..... | 20 |
| 3. Schematic of a typical polar of an aircraft. | 21 |
| 4. Ratio $E = C_L/C_D$ as a function of lift coefficient (schematic) | 21 |
| 5. Lift coefficient as a function of angle of attack and flap deflection (schematic). | 22 |
| 6. Airplane polar as a function of flap deflection (schematic). | 22 |
| 7. Typical change in $\Delta C_{L_{max}}(\delta)$ and $\Delta C_{L_0}(\delta)$ as a function of δ (schematic)..... | 23 |
| 8. Shock formation (schematic). | 24 |
| (a) Subsonic flow over entire airfoil..... | 24 |
| (b) Critical Mach number..... | 24 |
| (c) Supercritical Mach number..... | 24 |
| (d) Transonic Mach number..... | 24 |
| 9. Influence of trailing-edge deflection on profile pressure distribution and weak shock wave (schematic)..... | 25 |
| (a) Faired trailing edge ($\delta = 0$)..... | 25 |
| (b) Trailing-edge-down deflection. | 25 |
| 10. Polar of aircraft for transonic field (schematic). | 26 |
| 11. Drag coefficients as a function of Mach number and trailing-edge (flap) deflection (schematic). | 26 |
| 12. Minimum drag coefficient as a function of Mach number (schematic). | 27 |
| 13. Efficiency factor K as a function of Mach number (schematic) | 27 |
| 14. Wave drag coefficient as a function of Mach number and C_L (schematic). | 28 |
| 15. Variation of wing drag coefficient with Mach number (schematic)..... | 28 |
| 16. Polar of airplane as a function of the flap deflection (schematic)..... | 29 |
| 17. Variation of drag polar as a function of trailing-edge deflection (schematic). | 29 |
| 18. The L-1011 airplane. | 30 |
| 19. Real and parabolic polar of the L-1011 airplane for Mach 0.60 and Mach 0.83. | 30 |

| | |
|--|----|
| 20. Decrement of minimum drag coefficient as a function of trailing-edge (flap) deflection.. | 31 |
| 21. Nonparabolic variation of drag coefficient. | 31 |
| (a) Decrement of drag coefficient ($C_{L_{max}} - C_L$). | 31 |
| (b) Decrement of drag coefficient as a function of trailing-edge (flap) deflection. | 32 |
| 22. Decrement of the lift coefficient as a function of the trailing-edge (flap) deflection. | 32 |
| 23. Increment of wave drag coefficient as a function of the lift coefficient and Mach number. | 33 |
| 24. Increment of the critical lift coefficient as a function of Mach number and trailing-edge (flap) deflection. | 33 |
| 25. Incremental pitching moment from variable camber (flat-plate flap) from typical airfoil (NASA 23012). | 34 |
| 26. Correction on real polar for Mach 0.60. | 34 |
| 27. Correction on real polar for Mach 0.83. | 35 |
| 28. A family of polars of the L-1011 aircraft with variable camber for different deflection of trailing-edge angles and Mach 0.60. | 35 |
| 29. Relation of L/D variation with C_L for a range of trailing-edge deflections. | 36 |
| 30. Incremental $\Delta L/D$ performance benefit variation with trailing-edge deflections. | 36 |
| 31. Maximum increment of $\Delta L/D$ benefit at Mach 0.60. | 37 |
| 32. Optimal angle of trailing edge at Mach 0.60 (outer locus of fig. 30). | 37 |
| 33. A family of polars for different deflections of trailing-edge angles at Mach 0.83. | 38 |
| 34. Relation $E = C_L/C_D$ for different flap deflections at Mach 0.83. | 38 |
| 35. Increment ΔE (percent) for different flap deflection at Mach 0.83. | 39 |
| 36. Maximum increment $\Delta L/D$ benefit at Mach 0.83. | 39 |
| 37. Optimal angle of trailing edge. | 40 |

ABSTRACT

Analytical benefits of variable-camber capability on subsonic transport aircraft are explored. Using aerodynamic performance models, including drag as a function of deflection angle for control surfaces of interest, optimal performance benefits of variable camber are calculated. Results demonstrate that if all wing trailing-edge surfaces are available for optimization, drag can be significantly reduced at most points within the flight envelope. The optimization approach developed and illustrated for flight uses variable camber for optimization of aerodynamic efficiency (maximizing the lift-to-drag ratio). Most transport aircraft have significant latent capability in this area. Wing camber control that can affect performance optimization for transport aircraft includes symmetric use of ailerons and flaps. In this paper, drag characteristics for aileron and flap deflections are computed based on analytical and wind-tunnel data. All calculations based on predictions for the subject aircraft and the optimal surface deflection are obtained by simple interpolation for given conditions. An algorithm is also presented for computation of optimal surface deflection for given conditions. Benefits of variable camber for a transport configuration using a simple trailing-edge control surface system can approach more than 10 percent, especially for nonstandard flight conditions. In the cruise regime, the benefit is 1–3 percent.

NOMENCLATURE

Symbols

| | |
|----------------------------------|--|
| \bar{c} | mean aerodynamic chord, ft |
| c_1 | specific fuel consumption, min^{-1} |
| C_D | drag coefficient |
| $C_{D_{\text{analytical}}}$ | analytical drag coefficient in a given area |
| C_{D_i} | induced drag coefficient |
| C_{D_m} | balance drag |
| \bar{C}_{D_m} | relative balance drag, C_{D_m}/C_D |
| $C_{D_{\text{min}}}(\delta)$ | $C_{D_{\text{min}}}$ for $\delta \neq 0$ |
| $C_{D_{\text{min}}}(\delta = 0)$ | $C_{D_{\text{min}}}$ for $\delta = 0$ |
| $C_{D_{\text{test}}}$ | drag coefficient from wind-tunnel test |
| C_L | aircraft lift coefficient |
| $C_{L_{\text{max}}}$ | maximum wing lift coefficient |
| $C_{L_{\text{max}}}(\delta)$ | $C_{L_{\text{max}}}$ for $\delta \neq 0$ |
| $C_{L_{\text{max}}}(\delta = 0)$ | $C_{L_{\text{max}}}$ for $\delta = 0$ |
| $C_{L_{\text{min}}}$ | minimum wing lift coefficient |
| C_{L_o} | lift coefficient in point $C_{D_{\text{min}}}$ |
| $C_{L_o}(\delta = 0)$ | C_{L_o} for $\delta = 0$ |
| C_m | pitching-moment coefficient |

| | |
|----------------------------|--|
| C_p | pressure coefficient |
| D | drag force, lbf |
| E | aerodynamic efficiency ($E = L/D = C_L/C_D$) |
| \bar{E} | change in E , percent |
| E_o | ratio of C_L to C_D for $\delta = 0$ |
| K | efficiency factor in formula of induced drag |
| L | lift force, lbf |
| L/D | lift-to-drag ratio |
| M | Mach number |
| M_{cr} | critical Mach number |
| M_∞ | free-stream Mach number |
| p | air pressure in given point, lbf/ft ² |
| p_∞ | free-stream static pressure, lbf/ft ² |
| q | dynamic pressure, lbf/ft ² |
| Re | Reynolds number |
| S | wing platform area, ft ² |
| S_t | stabilizer platform area, ft ² |
| T | thrust, lbf |
| W | gross weight, lb |
| w_f | fuel consumption rate, lb/min |
| \bar{w}_f | change in fuel consumption, percent |
| x | distance from leading edge, ft |
| X | distance between the ($\bar{c}/4$) wing and ($\bar{c}/4$) stabilizer, ft |
| α | angle of attack, deg |
| δ | flap angle or deflection of trailing edge (positive is down), deg |
| Δ | change |
| ΔC_{D_c} | correction of parabolic polar |
| $\Delta C_{D_{np}}$ | increment of C_D between parabolic variation and nonparabolic variation for high and low lift coefficients |
| $\Delta C_{D_{np}L_{max}}$ | increment of C_D for region near $C_{L_{max}}$ |
| $\Delta C_{D_{np}L_{min}}$ | increment of C_D for region near $C_{L_{min}}$ |
| $\Delta C_{D_{wave}}$ | additional wave drag coefficient for ($M > M_{cr}$) |
| $\Delta C_{L_o}(\delta)$ | change of coefficient C_{L_o} in point $C_{D_{min}}$ from angle of trailing edge |

| | |
|------------------------------|---|
| $\Delta C_{L_{\text{wave}}}$ | change in C_L where wave drag appears |
| ΔM | additional pitching moment from trailing edge |

Subscripts

| | |
|------|-----------------|
| max | maximum |
| min | minimum |
| opt | optimum |
| t | horizontal tail |
| wing | wing |

INTRODUCTION

Aircraft efficiency is an important factor for airline operation. Fuel costs can approach 50 percent of airline operating expense for some modern, wide-body, long-range transports. A 3-percent reduction of fuel consumption can produce savings of as much as \$300,000/yr for each aircraft.¹ Variable-camber control of the wing for drag reduction throughout the flight mission using existing control surfaces can provide the ability to realize these savings. Variable camber is ideally suited for future aircraft because the available control surfaces can be used throughout the flight envelope: flaps used for takeoff and landing and ailerons used for routine turning maneuvers can be used in combination to provide variable-camber control during cruise flight. In addition to these savings, reduced fuel consumption results in equivalent reductions in atmospheric gas emissions, which is an increasingly important environmental issue.

Many issues enter into performance optimization for transport aircraft.²⁻⁵ Foremost, the potential for optimization must exist, which implies redundant control effect capability (that is, more than one means of trimming the forces and moments to obtain a steady-state flight condition). Most transport aircraft have significant capability in this area; taking maximum advantage of this capability is the theme of this paper. Controls and variables that potentially can play a role in performance optimization for current- and future-generation transport aircraft include the elevator, horizontal stabilizer, outboard aileron, inboard aileron, flaps, slats, rudder, center of gravity, and differential thrust.

The Advanced Fighter Technology Integration (AFTI)/F-111 Mission Adaptive Wing (MAW) program developed and demonstrated the potential of using variable-camber control to optimize cruise and maneuver flight conditions for fighter configurations.^{6, 7} In general, the objective was to have the ability to actively modify airfoil camber, spanwise camber distribution, and wing sweep in flight while maintaining a smooth and continuous airfoil surface. Features of the mission adaptive wing included cruise camber control to maximize vehicle efficiency during straight and level flight; maneuver camber control; maneuver load control; and maneuver enhancement and gust alleviation.

Preliminary design work has been performed for implementing variable camber into the A-330/340 transport and other aircraft.² In addition, numerous reports document trajectory optimization algorithms and their benefits relative to the economics of commercial transports.^{4, 5} In fact, all large transports

currently being produced have onboard flight management systems that “optimize” the aircraft trajectory to minimize cost as a function of flight time and fuel price.⁸ However, the commonality of all these algorithms is that the model used for performance optimization is the predicted base configuration; no ability exists to use variable-geometry features that are available with redundant control surfaces.

NASA Dryden Flight Research Center (Edwards, California) has developed drag-reduction technologies for transport aircraft. The realizable performance benefits typically are smaller for transport aircraft than for fighter aircraft, and as such, the task is challenging. These technologies include the application of measurement-based optimum control for performance improvement using variable-geometry concepts (redundant control effects). For example, symmetric aileron deflection can be applied to optimally recamber the wing to minimize drag for all aircraft configurations and flight conditions.¹

For fly-by-wire transports, the modification can be as simple as loading new flight management system and control display unit software. Transport aircraft with mechanical systems additionally require relatively simple control hardware modifications.

This analytical study explores the potential benefits of variable-camber capability on subsonic transport aircraft. Using aerodynamic performance models of the aircraft, including control-surface drag effects, optimum performance benefits of variable camber can be calculated. The optimization (maximizing the lift-to-drag ratio, L/D) typically is minimization of aircraft drag for various aircraft configurations and flight conditions. This paper presents a method for computing optimally predicted surface deflection for given flight conditions and predicted drag characteristics for aileron and flap deflections based on analytical and wind-tunnel data.

WING CAMBER CONTROL BACKGROUND

The Wright brothers’ attempt to alter lift characteristics using wing warping may be viewed as the first practical application of varying camber. Subsequent aircraft designs have employed leading- and trailing-edge devices to improve low-speed takeoff and landing performance. The challenge, however, is to include cruise flight in the variable-camber concept in order to maximize the benefits of having a full-envelope variable-camber capability.¹⁻³

Current subsonic-transport design results in a point-design configuration with the exception of flap usage at low-speed flight conditions. By necessity, the final configuration is a major compromise among a multitude of design considerations. Additional operational constraints include air-traffic-control directives (speed and altitude), loading (cargo and fuel), center of gravity, flight length, variations in manufacturing, aging, and asymmetries.³

Current-generation aircraft have a wide range of control surfaces that can be adapted to provide varying degrees of variable-camber capability. These surfaces include the elevator, horizontal stabilizer, outboard aileron, inboard aileron, outboard flaps, and inboard flaps.

Mechanical and software changes would be required to implement variable camber in current-generation aircraft, and some surfaces are significantly simpler to use than others. Ideally, variable camber should be designed into the aircraft rather than retrofitted. Such a design would have benefits because the aerodynamic tailoring would be optimized for application of variable camber. A variable-camber aircraft will be modestly more complex than current-generation aircraft.^{6, 7, 9, 10}

ANALYTICAL DEVELOPMENT OF VARIABLE-GEOMETRY WING CAMBER OPTIMIZATION

The equations describing the influence of camber in the calculated performance of a generic-transport wing profile are developed based on theoretical concepts and wind-tunnel data. The equations for lift and drag coefficients are expanded to include all effects for a typical transport wing. The application of the variable-camber feature is noted as the development progresses. Emphasis is placed on showing the effects of variable camber.

Development of Low-Speed Lift and Drag Coefficient Expressions as a Function of Camber

Aircraft lift coefficient (C_L) and drag coefficient (C_D) can be defined as

$$C_L = L/qS \quad (1)$$

and

$$C_D = D/qS. \quad (2)$$

Lift and drag coefficients are complex functions of profile shape, angle of attack (α), wing planform (S), Mach number (M), Reynolds number (Re), and so forth. These functions may be found from computation, wind-tunnel testing, or flight testing.

The aerodynamic results are typically presented as graphs of

$$C_L = f(\alpha), \quad (3)$$

$$C_D = f(\alpha), \quad (4)$$

and

$$C_D = f(C_L). \quad (5)$$

Figures 1–3 show typical variations of these functions for low-speed (no shock wave) flight. In the region where the C_L variation with α is approximately linear, the curves of equations (4) and (5) have parabolic shape. A very important characteristic of transport aircraft is the maximum L/D achievable in cruise flight,

$$L/D = C_L/C_D, \quad (6)$$

which figure 4 shows as a function of C_L . The objective of performance optimization is to maximize the L/D at all cruise flight conditions.

For low speed (less than Mach 0.6), the formula of C_D can be approximated by

$$C_D = C_{D_{\min}} + C_{D_i}, \quad (7)$$

where $C_{D_{\min}}$ is the minimum of C_D , and C_{D_i} is drag induced by the lift force. The C_{D_i} can be approximated by

$$C_{D_i} = K(C_L - C_{L_o})^2, \quad (8)$$

where C_{L_o} is the lift coefficient in point $C_{D_{\min}}$ (fig. 3), and K is the efficiency factor. In particular, K depends on the aspect ratio of the wing and Mach number.

Outside of the parabolic region, the nonparabolic variations can be found using wind-tunnel testing. An expression for C_D over the full range of C_L is:

$$C_D = C_{D_{\min}} + C_{D_i} + \Delta C_{D_{np}}(C_L), \quad (9)$$

where $\Delta C_{D_{np}}$ is the increment of C_D between the parabolic variation and the nonparabolic variation for high and low lift coefficients—in other words, the increment of C_D in regions near $C_{L_{\max}}$ and $C_{L_{\min}}$ (figs. 1 and 3):

$$\Delta C_{D_{np}} = \Delta C_{D_{np}L_{\max}} \quad (10)$$

or

$$\Delta C_{D_{np}} = \Delta C_{D_{np}L_{\min}}. \quad (11)$$

Influence of Shape on Aerodynamics

The wing trailing edge has a strong influence on the aerodynamics of a given wing profile. In the subsonic region, increasing camber (increasing downward flap deflection, δ) requires less α for a fixed C_L , or increases the coefficient C_L for a constant α (fig. 5).¹¹ The linear region of C_L as a function of α is also increased to a larger C_L . The maximum C_L also increases (fig. 5):

$$C_{L_{\max}}(\delta) = C_{L_{\max}}(\delta = 0) + \Delta C_{L_{\max}}(\delta). \quad (12)$$

The coefficient $C_{D_{\min}}$ increases (fig. 6) by the relation

$$C_{D_{\min}}(\delta) = C_{D_{\min}}(\delta = 0) + \Delta C_{D_{\min}}(\delta). \quad (13)$$

The flap deflection changes the lift coefficient for minimum drag C_{L_o} by the amount $\Delta C_{L_o}(\delta)$ (fig. 6). The coefficient C_{L_o} equals

$$C_{L_o}(\delta) = C_{L_o}(\delta = 0) + \Delta C_{L_o}(\delta), \quad (14)$$

where $\Delta C_{L_o}(\delta)$ is the change in C_{L_o} caused by trailing-edge deflection (fig. 6). Figure 7 shows typical variations of the $\Delta C_{L_o}(\delta)$ and $\Delta C_{L_{\max}}(\delta)$ as a function of δ .

Influence of Mach Number on Aerodynamics

For high-speed (transonic) flight (Mach 0.6–0.9), development of a normal shock wave on the upper airfoil surface results in additional drag effects (fig. 8). At speeds faster than the critical Mach number (M_{cr}), where the velocity of certain regions on the upper surface reach the speed of sound, the coefficients C_L , C_D , and K also depend on Mach number. The critical Mach number, typically between Mach 0.6 and 0.8, depends on the airfoil profile and the position of the profile to the direction of flow (angle of attack of the wing).

Camber or flap deflection also influences the critical Mach number. A nonsupercritical profile (without flap deflection) may incur supercritical properties with a slight flap deflection. In this case, the pressure coefficient (C_p) distribution of the surface profile is changed (fig. 9):

$$C_p = (p - p_\infty)/q. \quad (15)$$

The maximum C_p is decreased and a strong shock wave becomes a weak shock wave for small camber increases. As a result, the critical Mach number increases.

When the Mach number is greater than the critical Mach number, C_D increases by the additional wave drag increment, $\Delta C_{D_{\text{wave}}}$ (fig. 10).

$$\Delta C_{D_{\text{wave}}} = \Delta C_{D_{\text{wave}}}((C_L - \Delta C_{L_{\text{wave}}}(M, \delta)), M) \quad (16)$$

The $\Delta C_{D_{\text{wave}}}$ depends on the $C_L(\alpha)$ of the wing in the transonic speed regime. For small lift coefficients, figure 10 shows the drag form is approximately parabolic in the transonic range from point A to point B. For lift coefficients greater than point B at transonic speeds, a normal shock wave develops that produces an additional wave drag component [$C_D = f(C_L)$, which departs from an approximately parabolic curve (fig. 10) when the C_L is greater than point B]. After adding equations (13) and (16), equation (9) now has a form

$$C_D = C_{D_{\min}} + C_{D_i} + \Delta C_{D_{\text{np}}} + \Delta C_{D_{\min}} + \Delta C_{D_{\text{wave}}}. \quad (17)$$

For $\delta > 0$, the point where $C_D = f(C_L)$ departs from a parabola is increased by the value

$$\Delta C_{L_{\text{wave}}} = \Delta C_{L_{\text{wave}}}(M, \delta). \quad (18)$$

Note that the break from parabolic shape caused by the shock wave can occur in the linear region of $C_L(\alpha)$.

Figures 11–16 show typical variations of C_D , $C_{D_{\min}}$, K , $\Delta C_{L_{\text{wave}}}$, and $\Delta C_{D_{\text{wave}}}$ as a function of M and M_{cr} . Figure 17 shows typical polars as a function of δ .

Influence of Pitching Moments on Aerodynamics

The cambering effects, discussed in previous sections, also introduce pitching-moment effects that require aircraft retrimming using the horizontal tail. A positive increase in camber on the wing normally produces a negative pitching moment, which in turn must be balanced by a negative lift force at the horizontal tail that produces a moment tending to cancel the moment from the wing cambering. Consequently, the wing must produce an additional positive lift force for a fixed weight condition. The additional positive lift force produces additional induced drag. The benefit from variable camber will thus decrease.

An estimate of the effects that pitching moments have on the performance benefits of variable camber is derived as follows: The additional pitching moment caused by flap deflection is

$$\Delta M = \Delta C_m q S \bar{c}, \quad (19)$$

where ΔC_m is the pitching-moment coefficient increment. This moment must be balanced by an additional moment of horizontal tail,

$$\Delta M_t = \Delta L_t X = \Delta C_{L_t} q S_t X, \quad (20)$$

where the tail lift force is

$$\Delta L_t = \Delta C_{L_t} q S_t \quad (21)$$

and X is the distance between the $(\bar{c}/4)$ wing and $(\bar{c}/4)$ stabilizer.

Setting equations (19) and (20) equal,

$$\Delta C_{L_t} = \Delta C_m S \bar{c} / (S_t X). \quad (22)$$

The increase in wing lift can be expressed as

$$\Delta L_{\text{wing}} = \Delta C_L q S. \quad (23)$$

Summing equations (21) and (23) and setting them equal to 0 yields

$$\Delta C_L = -\Delta C_{L_t} S_t / S. \quad (24)$$

Because the induced drag coefficient of the wing is

$$C_{D_i} = K(C_L - C_{L_o})^2,$$

the incremental drag coefficient caused by pitching-moment effects is

$$\Delta C_{D_m} = C_{D_i}(\text{with flaps}) - C_{D_i}(\text{no flaps}) = K(C_L + \Delta C_L - C_{L_o})^2 - K(C_L - C_{L_o})^2.$$

Simplifying the above yields

$$\Delta C_{D_m} = K[2\Delta C_L(C_L - C_{L_o}) + \Delta C_L^2]. \quad (25)$$

Substituting equation (22) into equation (24) produces

$$\Delta C_L = -\Delta C_m \bar{c} / X. \quad (26)$$

Substituting equation (26) into equation (25) produces

$$\Delta C_{D_m} = K \left[-2\Delta C_m (C_L - C_{L_o}) \bar{c} / X + (\Delta C_m \bar{c} / X)^2 \right]. \quad (27)$$

This term then is added to the previous drag expression of equation (18). The percentage of drag change, $\Delta \bar{C}_{D_m}$, of ΔC_{D_m} to the C_D of equation (18) is

$$\Delta \bar{C}_{D_m} = (\Delta C_{D_m} / C_D) \cdot 100 \text{ percent}. \quad (28)$$

General Correction for Nonparabolic Polar

The drag equation development has assumed a parabolic shape to the point of wave drag occurring. If wind-tunnel data are available in the region of low lift coefficients and indicate a nonparabolic drag polar, a correction term can be added for the difference between the assumed parabolic shape and the wind-tunnel data (fig. 3). This correction term can be expressed as

$$\Delta C_{D_c} = \Delta C_{D_c}(C_L). \quad (29)$$

Summary of Equations

Summarizing the derivation of C_D by substituting the terms from equations (9)–(11), (16), (17), (27), and (29), the aircraft drag coefficient can be rewritten as:

$$C_D = C_{D_{\min}}(\delta = 0) + \Delta C_{D_{\min}}(\delta) + \Delta C_{D_{np}}(C_L, \delta) + C_{D_i}(C_L, C_{L_o}(\delta), M) \\ + \Delta C_{D_{\text{wave}}}[C_L - \Delta C_{L_{\text{wave}}}(M, \delta), M] + \Delta C_{D_m}(C_L, \delta) + \Delta C_{D_c}(C_L). \quad (30)$$

C_D is the total drag, $C_{D_{\min}} (\delta = 0)$ is the minimum of drag coefficient (figs. 2 and 3), and $\Delta C_{D_{\min}} (\delta)$ is the increment minimum drag coefficient from flap (eq. (13) and fig. 6).

$$\Delta C_{D_{np}} = \Delta C_{D_{npL_{\max}}} (C_L) + \Delta C_{D_{npL_{\min}}} (C_L, \delta),$$

where $\Delta C_{D_{npL_{\max}}} (C_L)$ is the increment C_D in region $C_{L_{\max}}$ (eq. (10)) and $\Delta C_{D_{npL_{\min}}} (C_L, \delta)$, is the increment C_D in the region $C_{L_{\min}}$ (eq. (11) and fig. 3).

C_{D_i} , the induced drag coefficient (eqs. (8) and (14) and fig. 3), is

$$C_{D_i} = K(M) \cdot (C_L - C_{L_o} (\delta = 0) - \Delta C_{L_o} (\delta))^2, \quad (31)$$

where $K(M)$ is the efficiency coefficient (eq. (8)); and $\Delta C_{L_o} (\delta)$ is the change coefficient C_{L_o} , which depends on the angle of deflection, δ (fig. 6).

$$\Delta C_{D_{wave}} [(C_L - \Delta C_{L_{wave}} (M, \delta)), M]$$

is the increment of drag coefficient from (M, δ) in equation (16).

$\Delta C_{L_{wave}} (M, \delta)$ is the increment of lift coefficient from change pressure distribution (eq. (16) and fig. 16).

$$\Delta C_{D_m} = K \left[-2\Delta C_m (C_L - C_{L_o}) \bar{c}/X + (\Delta C_m \bar{c}/X)^2 \right] - \text{balance drag (eq. (27))}.$$

$$C_{L_o} = C_{L_o} (\delta = 0) + \Delta C_{L_o} (\delta), \quad (32)$$

and $\Delta C_{D_c} (C_L)$ is the correction of the parabolic polar to the real polar for a few lift coefficients.

Influence of the Lift-to-Drag Ratio on Fuel Consumption

Fuel consumption is proportional to the aircraft total thrust:

$$w_f = c_1 T, \quad (33)$$

where w_f is the fuel consumption rate, T is the thrust of all airplane engines, and c_1 is the specific fuel consumption and is assumed constant at cruise conditions. At stabilized cruise conditions,

$$T = W/E. \quad (34)$$

Substituting equation (34) into equation (33),

$$w_f = c_1 W/E, \quad (35)$$

where $E = L/D = C_L/C_D$. Find dw_f/dE :

$$dw_f = -c_1 W dE/E^2. \quad (36)$$

Noting that

$$d\bar{w}_f = (dw_f/w_f) \cdot 100 \text{ percent} = (dw_f E/c_1 W) \cdot 100 \text{ percent}, \quad (37)$$

then

$$d\bar{E} = (dE/E) \cdot 100 \text{ percent}. \quad (38)$$

The percent of fuel consumption is related to the percent of the aerodynamic efficiency L/D as

$$d\bar{w}_f = -d\bar{E}. \quad (39)$$

CALCULATION OF VARIABLE-CAMBER BENEFITS FOR A TYPICAL WIDE-BODY TRANSPORT

As observed from equations (1)–(39), the aerodynamics of a variable-camber configuration using only trailing-edge control surfaces are complex and depend on factors such as trailing-edge deflection, Mach number, and so forth. This section expands on the theoretical development of the previous section and develops the example database from which the variable-camber benefits can be calculated. Figure 18 shows the L-1011 transport (Lockheed Corporation, Burbank, California) selected as a representative aircraft to demonstrate the benefits of variable camber.

Database Development

This section develops an appropriate database. The available L-1011 data do not contain many of the required parameters; thus, these parameters were obtained from other sources. Using flight data would be ideal; lacking that, wind-tunnel or analytical data must be used. This section takes the terms of equation (30) and discusses the development of the database for each term. The database developed in this section is then used to calculate benefits that will be discussed in the next section.

C_D

The term C_D is obtained from unpublished L-1011 flight results. For this report, two conditions are analyzed: Mach 0.60 for climb and descent regimes, and Mach 0.83 for cruise conditions. Figure 19 shows polars for these two conditions.

The approximate parabolic region used for this analysis is as follows:

$$\begin{aligned} \text{Mach 0.60: } C_L &= 0.12\text{--}0.60 \\ \text{Mach 0.83: } C_L &= 0.12\text{--}0.50 \end{aligned} \quad (40)$$

Assuming a parabolic polar form of

$$C_D = C_{D_{\min}} + K(C_L - C_{L_o})^2, \quad (41)$$

a fit of the data (fig. 19) yields values of $C_{D_{\min}}$, K , and C_{L_o} for regions defined by equation (40). These values are as follows:

$$\text{Mach 0.60: } C_{D_{\min}} = 0.0165 \quad K = 0.0832 \quad C_{L_o} = 0.12 \quad (42)$$

$$\text{Mach 0.83: } C_{D_{\min}} = 0.018 \quad K = 0.10547 \quad C_{L_o} = 0.16 \quad (43)$$

Figure 19 also shows the parabolic fits.

$\Delta C_{D_{\min}}(\delta)$

The term $\Delta C_{D_{\min}}$ represents how the minimum drag coefficient varies with respect to trailing-edge control surface deflection, δ (fig. 20). The term is calculated based on empirical data and techniques¹⁰ using a correction for smooth surface and data obtained from reference 12. The term is assumed to be independent of Mach number.

$\Delta C_{D_{np}}$

At extreme values of C_L , the actual drag polar begins to deviate and continues to deviate significantly from the ideal parabolic variation (fig. 3). The variations at the extreme lift coefficients are estimated based on empirical data and techniques of reference 10 and are shown in figure 21. For maximal lift coefficients, $C_{L_{\max}}(\delta)$ is determined:

$$C_{L_{\max}}(\delta) = C_{L_{\max}}(\delta = 0) + \Delta C_{L_{\max}}(\delta),$$

where $\Delta C_{L_{\max}}(\delta)$ is obtained from figure 22 and $C_{L_{\max}}(\delta = 0)$ is obtained from a lift curve slope as indicated in figure 1.

The C_L of interest is subtracted from $C_{L_{\max}}$; the $\Delta C_{D_{np}}$ (fig. 21(a)) is then obtained from the curve. This value is not a function of trailing-edge deflection, and no correction exists for $C_{L_{\max}} - C_L > 0.1$ (fig. 21(a)).

For minimal lift coefficients, the $C_{D_{np}}$ is read directly from figure 21(b) as a function of C_L and flap deflection, δ . These values were estimated by the method described in reference 10.

$\Delta C_{L_{\max}}$ is the maximum lift coefficient obtainable with trailing-edge control surface deflections. This value is calculated by the method described in reference 10 (also refer to reference 13, chapter 3 and reference 14). These terms are assumed to be independent of Mach number.

C_{D_i}

The term C_{D_i} represents the induced drag caused by C_L (or angle-of-attack) variation:

$$C_{D_i} = K(C_L - C_{L_o}(\delta = 0) - \Delta C_{L_o}(\delta))^2;$$

K and $C_{L_o}(\delta = 0)$ are defined in the $C_{D_{min}}(\delta = 0)$ section. C_L is the lift coefficient of interest, and $\Delta C_{L_o}(\delta)$ is the lift contribution caused by increased trailing-edge deflection (fig. 22). This lift contribution is calculated by the method described in reference 10 (also see references 9–11, 13, 15, and 16).

$\Delta C_{D_{wave}}$

As indicated earlier, the wave drag component is caused by the shock wave affecting the parabolic shape of the drag polar. The wave drag correction term as a function of Mach number and $(C_L - \Delta C_{L_{wave}})$ is obtained from figure 23; $\Delta C_{L_{wave}}$ as a function of Mach number and flap deflection is obtained from figure 24. The estimate is based on data in reference 9, pages 398–406; reference 8, pages 232–236; reference 15, pages 291–302; reference 13, page 107; and reference 11, pages 64–68.

ΔC_{D_m}

The drag correction to pitching-moment balancing of the horizontal tail (eq. 27) is:

$$\Delta C_{D_m} = K \left[-2\Delta C_m (C_L - C_{L_o}) \bar{c}/X + (\Delta C_m \bar{c}/X)^2 \right],$$

where ΔC_m is obtained from figure 25 as a function of flap deflection. ΔC_m is obtained from reference 10.

ΔC_{D_c}

This correction is the difference between the usual quadratic drag polar (eqs. (7) or (41)) and wind-tunnel or flight data and is defined as:

$$\Delta C_{D_c} = C_{D_{\text{test}}} - C_{D_{\text{analytical}}}.$$

Because the L-1011 database represents a combination of wind-tunnel and flight data, figures 26–27 show this correction for Mach 0.60 and Mach 0.83, respectively.

Calculation of Variable-Camber Benefit from Database

With both C_L and C_D now available, efficiency factors can be calculated. In this analysis, L/D will be used as the measure of efficiency and will also be denoted by E :

$$E = L/D = C_L/C_D. \quad (44)$$

The percentage change of the efficiency ratio is then

$$\bar{E} = [(E - E_o)/E_o] \cdot 100 \text{ percent}, \quad (45)$$

where $E_o = C_L/C_D$ at $\delta = 0$. The maximum efficiency is found by:

$$\bar{E}_{\text{max}} = \max_{\delta} \bar{E}(C_L, M, \delta) \text{ for fixed } C_L, M. \quad (46)$$

These calculations result in the optimum trailing-edge (flap) deflection, δ_{opt} , for maximum efficiency:

$$\delta_{\text{opt}} = f(C_L, M). \quad (47)$$

ESTIMATED BENEFITS OF VARIABLE CAMBER FOR THE L-1011 EXAMPLE

Based on equations (1)–(39) and the aerodynamic database developed for the L-1011 aircraft, drag polars as a function of the entire trailing-edge deflection are calculated, and then performance measures are determined from these drag polars. The calculations are performed for two Mach numbers: Mach 0.60, representing a climb or an off–design cruise point condition; and Mach 0.83, which is the design cruise point of the aircraft.

Low-Speed Flight (Mach 0.60)

Figure 28 shows the family of drag polars as a function of flap deflection for Mach 0.60. These polars have the classic quadratic shape because wave drag is not a factor at this Mach condition. The data for C_L as a function of C_D (fig. 28) are then used to develop the L/D variations (fig. 29) that are shown as a

function of C_L for a range of flap deflection. Figure 30 shows the percent of change in L/D for the various flap conditions relative to the 0° flap-deflection condition. Figure 30 shows L/D as a strong function of both C_L and flap deflection; note that essentially no variable-camber benefit is available at $C_L \approx 0.35$. Figure 31 shows the locus of maximal L/D obtainable.

Figure 32 shows the flap deflection required to attain the maximal L/D at a given C_L . The variation shows that for very low lift coefficients, a negative (trailing-edge-up) deflection is required to attain L/D improvements; whereas at lift coefficients greater than approximately 0.35, increasing flap deflection is required to attain the maximal L/D as the C_L increases. Cruise flight typically is in the C_L range of 0.40–0.50, and as such, the available L/D improvements produced by variable camber are rather modest and in the range of 1–3 percent. As noted earlier, the percent of reduction in fuel consumption is approximately equal to the percent of increase in L/D . The C_{D_m} effect was very small (approximately 3 percent) of the benefit.

Cruise Flight (Mach 0.83)

Figure 33 shows the family of drag polars as a function of flap deflection for Mach 0.83. Comparison with the drag polars of figure 28 reveals the drag polars for Mach 0.83 are much more complex. The transonic polar is more difficult to calculate because the drag has a complex dependency on Mach number in the transonic regime and the aerodynamic data describing the influence of variable camber on the polar are limited. A small, increasing deflection of trailing-edge surfaces at a constant C_L can decrease wave drag, thus delaying the increase of wave drag to a higher Mach number (fig. 9).

The data for C_L as a function of C_D (fig. 33) are used to develop the L/D variations (fig. 34), which are presented as a function of C_L for a range of flap deflection. Figure 35 shows the percent of change in L/D as a function of C_L for various flap conditions relative to the 0° flap-deflection condition. Figure 35 shows that essentially no variable-camber benefit is available at $C_L \approx 0.35$, very similar to the low-speed case. Figure 36 shows the locus of the maximal L/D as a function of C_L ; note that the benefit peaks out at $C_L \approx 1.0$.

Figure 37 shows the flap deflection required to attain the maximal L/D at a given C_L . The variation shows that for very low lift coefficients, a negative (trailing-edge-up) deflection is required to attain L/D improvements; whereas at lift coefficients greater than approximately 0.35, increasing flap deflection is required to attain the maximal L/D as the C_L increases. Cruise flight typically is in the C_L range of 0.40–0.50, and as such, the available L/D improvements produced by variable camber are rather modest and in the range of 1–3 percent. As noted earlier, the percent of reduction in fuel consumption is approximately equal to the percent of increase in L/D .

Application of Variable Camber

The methodology developed in this report assumes application to aileron-type trailing-edge surfaces, even in the span locations normally occupied by flaps. Although the benefits discussed in this report could be obtained with software changes in fly-by-wire aircraft for the aileron surfaces, major modifications would be required to develop a system to obtain small deflections for the flaps. Ideally, the

benefits of variable camber will be maximized with future-generation aircraft in which variable camber is included in the original design. These future designs could include leading-edge control and variable-camber features more revolutionary than the simple trailing-edge rotation discussed in this report.

The benefits of optimization using variable camber discussed in this report involve maximizing L/D ; this effect can then be used in various ways. For example, instead of saving fuel, the mission can be flown at a faster speed for the same fuel consumption a lesser speed flown without optimization has. Or, because less fuel is required for the mission, the fuel weight reduction can be exploited by increasing payload (and thus, revenue). Because 1 lb of payload can generate as much as 30 times the value of the cost of 1 lb of fuel, these benefits can be huge. For payload- or range-limited aircraft, small increases in L/D can mean large increases in revenue. The variable-camber benefits are not only applicable to commercial transport aircraft but also to military aircraft that quite often have very large operational flight envelopes, thereby increasing the potential for variable-camber benefits.

The concepts developed in this report can also be applied to supersonic transport-type configurations, fighter aircraft, and helicopters. In addition, the technology can be applied to any aerodynamic surface (propellers, large turbine blades, varieties of sails, and so forth).^{17–20}

CONCLUDING REMARKS

An analytical approach to assessing the potential benefits of variable camber on transport-category aircraft has been developed. The methodology uses the lift-to-drag ratio, L/D , as the performance parameter to be maximized. The aerodynamic model data required for actual calculations can be derived from flight test, wind-tunnel, or analytical sources. The methodology was evaluated using the L-1011 aerodynamic model, which is representative of the long-range, wide-body transports for which the application of variable camber would be most beneficial.

The evaluation of variable-camber benefits was conducted at two Mach numbers, Mach 0.60 and Mach 0.83, and assumed full-span wing trailing-edge deflection capability. At Mach 0.60, the benefit ranged from nearly 0 percent at a lift coefficient (C_L) of 0.35 to a maximum of 9–12 percent at a C_L range of 0.8–1.2. At nominal cruise flight conditions, the benefit is 1–3 percent. The higher C_L conditions of climb and descent may enable obtaining benefits of 4 percent or more.

For Mach 0.83, the benefit is 1–3 percent in the cruise regime. The benefits are greater (a maximum of 14 percent) in the region $C_L > 0.8$, but this region is not used for cruise flight. The percent of fuel consumption reduction essentially is equal to the percent of L/D increase at a given condition.

The pitching-moment effect on the L/D caused by wing cambering effects and associated horizontal tail trim changes are approximately –3 percent of the variable-camber benefit in cruise regime. The variable-camber benefits for nominal flight conditions are rather modest because commercial aircraft are designed to be optimized for these nominal conditions. As such, the potential clearly exists for large benefits as the aircraft is operated at conditions further from the nominal profile. Although operating under such conditions would be rather infrequent for commercial operations, military operations have a much broader flight envelope; thus, the potential exists for significant benefits.

The benefits resulting from the application of the variable-camber wing can be used to minimize fuel consumption, maximize speed, maximize loiter time, and so forth. The benefits calculated in this report

may not exactly duplicate what is seen in flight because of the inexact nature of the process. However, the benefits calculated accurately reflect trends and provide an indication of the type of benefits that might be seen.

*Dryden Flight Research Center
National Aeronautics and Space Administration
Edwards, California, July 13, 1999*

REFERENCES

1. Gilyard, Glenn B., Jennifer Georgie, and Joseph S. Barnicki, *Flight Test of an Adaptive Configuration Optimization System for Transport Aircraft*, NASA TM-1999-206569, 1999.
2. Szodruch, J. and R. Hilbig, "Variable Wing Camber for Transport Aircraft," *Progress in Aerospace Sciences*, vol. 25, 1988, pp. 297–328.
3. Gilyard, Glenn, *In-Flight Transport Performance Optimization: An Experimental Flight Research Program and an Operational Scenario*, NASA TM-97-206229.
4. Bolonkin, A. A., *New Methods of Optimization and Their Applications*, Moscow Highest Technical University named Bauman, Moscow, 1972.
5. Bolonkin, Alexander and Narendra Khot, "Method for Finding a Global Minimum," AIAA-94-4420, Jan. 1994.
6. Phillips, Paul W. and Stephen B. Smith, *AFTI/F-111 Mission Adaptive Wing (MAW) Automatic Flight Control System Modes Lift and Drag Characteristics*, AFFTC-TR-89-03, May 1989.
7. National Aeronautics and Space Administration, *Advanced Fighter Technology Integration F-111 Mission Adaptive Wing*, NASA CP-3055, 1989.
8. Jenkins, Darryl, ed., *The Handbook of Airline Economics*, McGraw-Hill, Washington D.C., 1995, pp. 223–234 and 367–378.
9. Ferris, James C., *Wind-Tunnel Investigation of a Variable Camber and Twist Wing*, NASA TN-D-8475, 1977.
10. Air Force Flight Dynamics Laboratory, Flight Control Division, *USAF Stability and Control DATCOM*, Wright-Patterson AFB, Ohio, Oct. 1960, Ch. 6.
11. McCormick, Barnes W., *Aerodynamics, Aeronautics, and Flight Mechanics*, 2nd ed., John Wiley & Sons, Inc., New York, 1995.
12. Riegels, Friedrich Wilhelm, *Aerofoil Sections: Results from Wind-Tunnel Investigations*, D. G. Randall, trans., Butterworths, London, 1961.
13. Lan, C. Edward and Jan Roskam, *Airplane Aerodynamics and Performance*, Roskam Aviation and Engineering Corporation, Ottawa, Kansas, 1981.
14. Raymer, Daniel P., *Aircraft Design: A Conceptual Approach*, American Institute of Aeronautics and Astronautics, Inc., Washington D.C., 1989.
15. Bertin, John J. and Michael L. Smith, *Aerodynamics for Engineers*, 3rd edition, Prentice Hall, New Jersey, 1998.
16. Kuethe, Arnold M. and Chuen-Yen Chow, *Foundations of Aerodynamics: Bases of Aerodynamic Design*, 4th edition, John Wiley & Sons, New York, 1986.

17. Awani, A. O., *Analysis of a Variable Camber Device for Helicopter Rotor Systems*, Dissertation, Kansas University, Lawrence, Kansas, Jan. 1981.
18. "The Tunny Rig Variable-Camber Wingsail," *Ship & Boat International*, vol. 37, no. 11, Nov. 1983, pp. 32–33.
19. Crigler, John L., *The Effect of Trailing-Edge Extension Flaps on Propeller Characteristics*, NACA ACR-L5A11, 1945.
20. Talay, Theodore A., *Introduction to the Aerodynamics of Flight*, NASA SP-367, 1975.

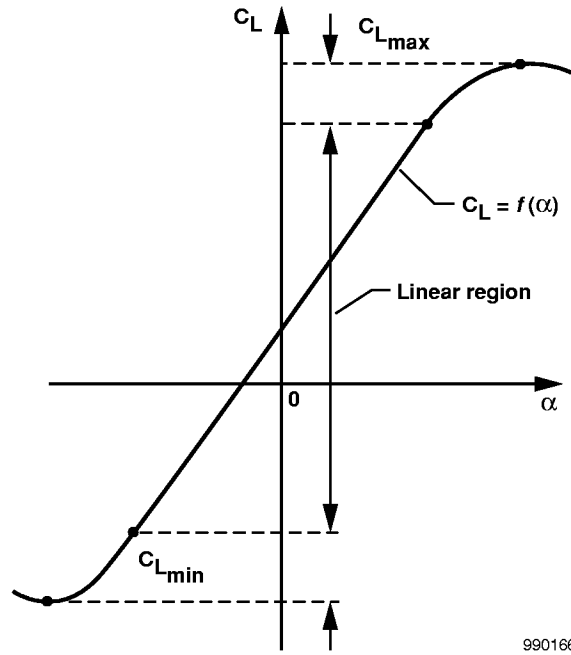


Figure 1. Lift coefficient plotted as a function of angle of attack (schematic).

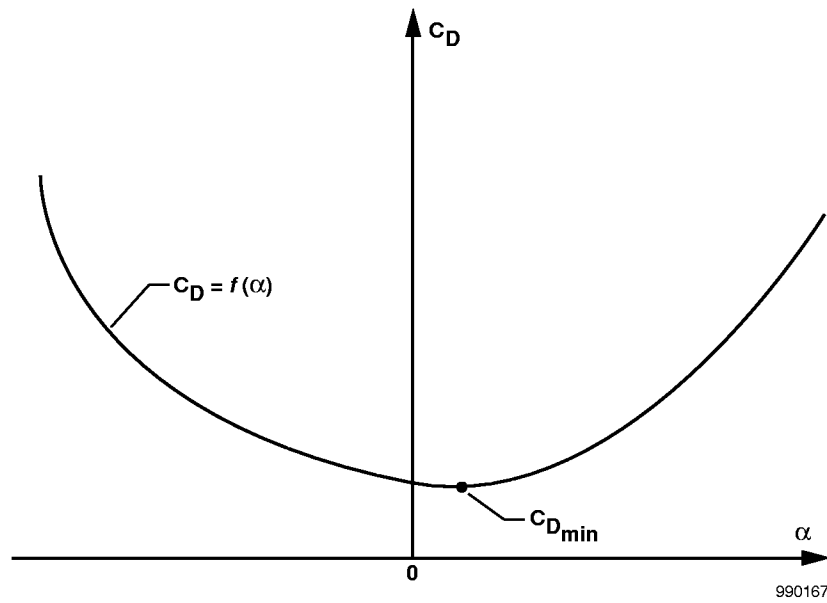
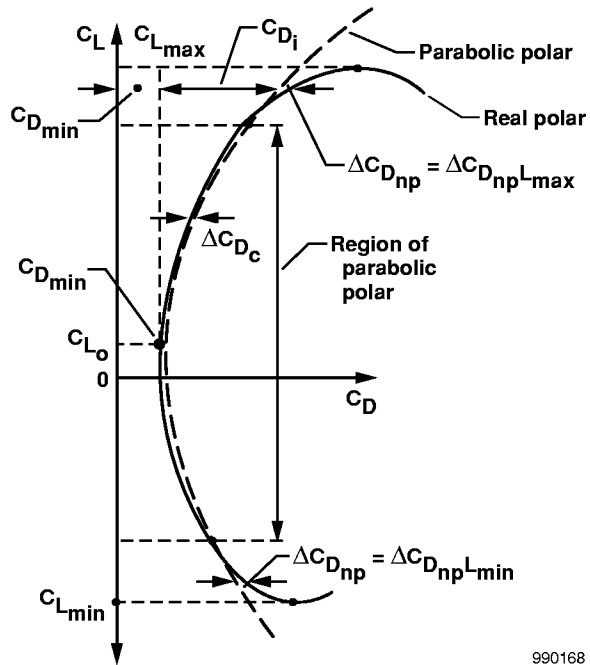
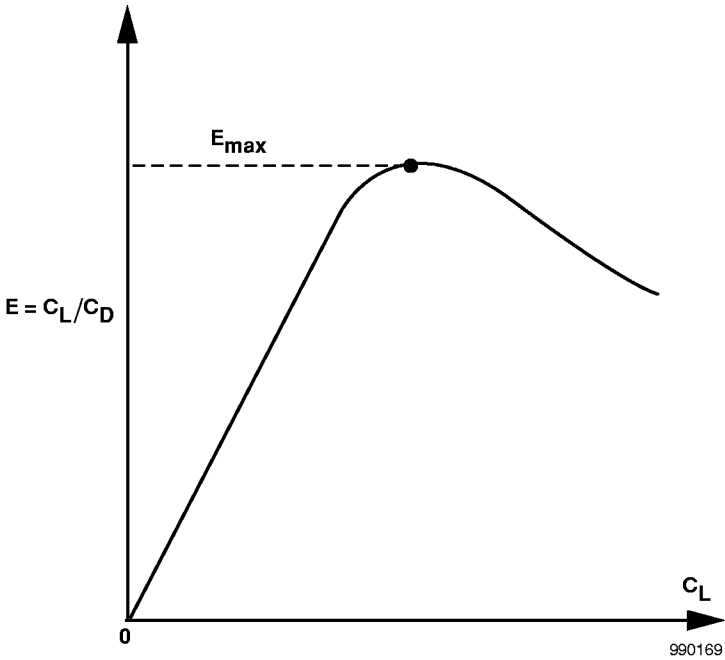


Figure 2. Drag coefficient plotted as a function of angle of attack (schematic).



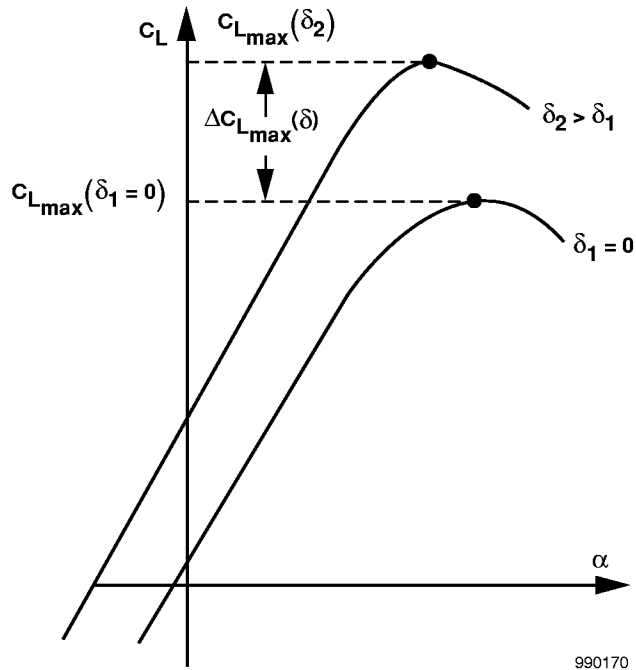
990168

Figure 3. Schematic of a typical polar of an aircraft.



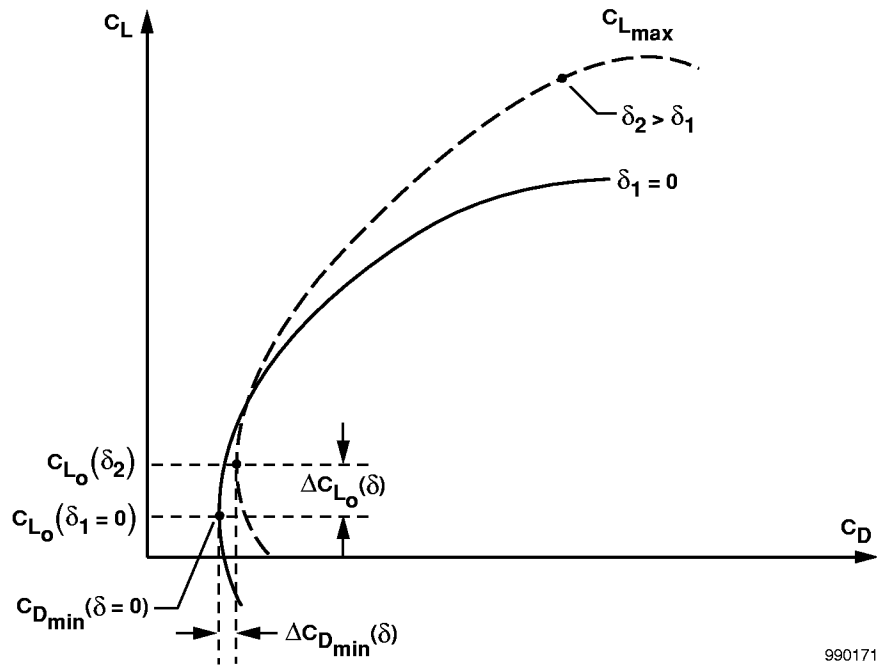
990169

Figure 4. Ratio $E = C_L / C_D$ as a function of lift coefficient (schematic).



990170

Figure 5. Lift coefficient as a function of angle of attack and flap deflection (schematic).



990171

Figure 6. Airplane polar as a function of flap deflection (schematic).

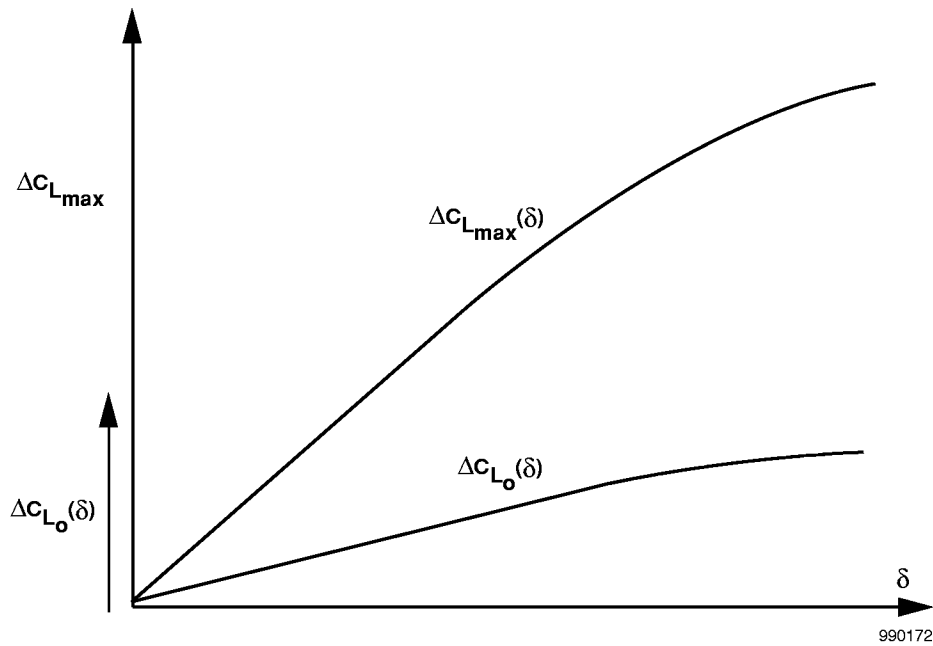
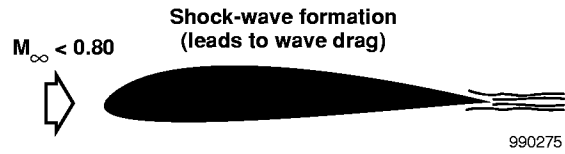
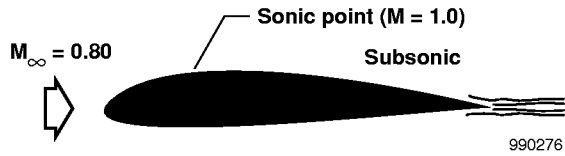


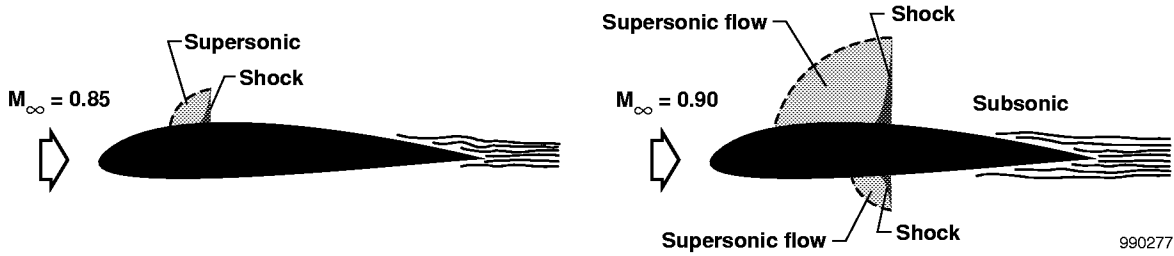
Figure 7. Typical change in $\Delta C_{L_{max}}(\delta)$ and $\Delta C_{L_o}(\delta)$ as a function of δ (schematic).



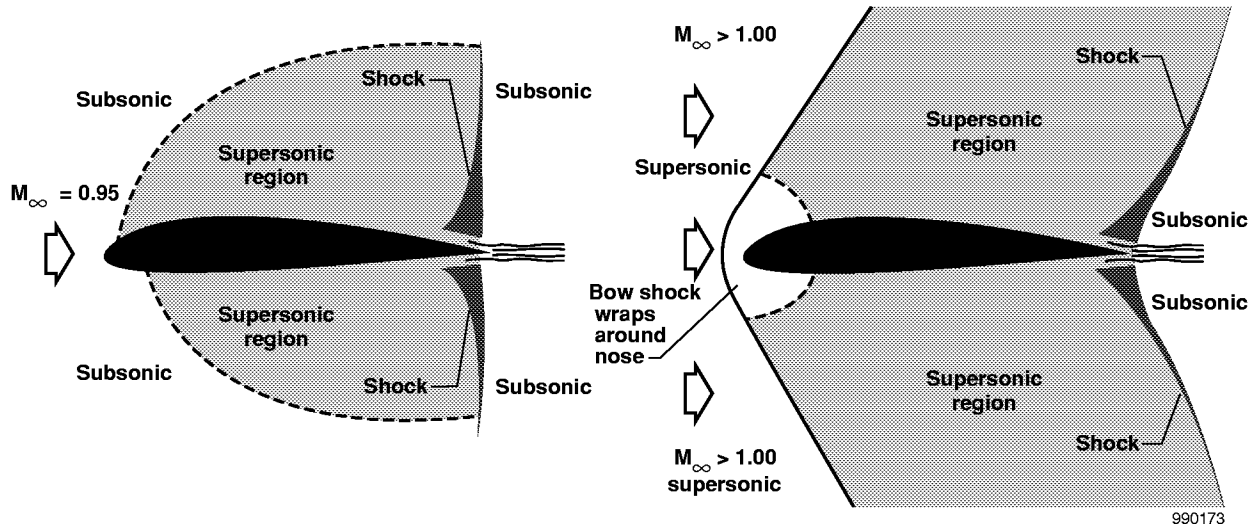
(a) Subsonic flow over entire airfoil.



(b) Critical Mach number.

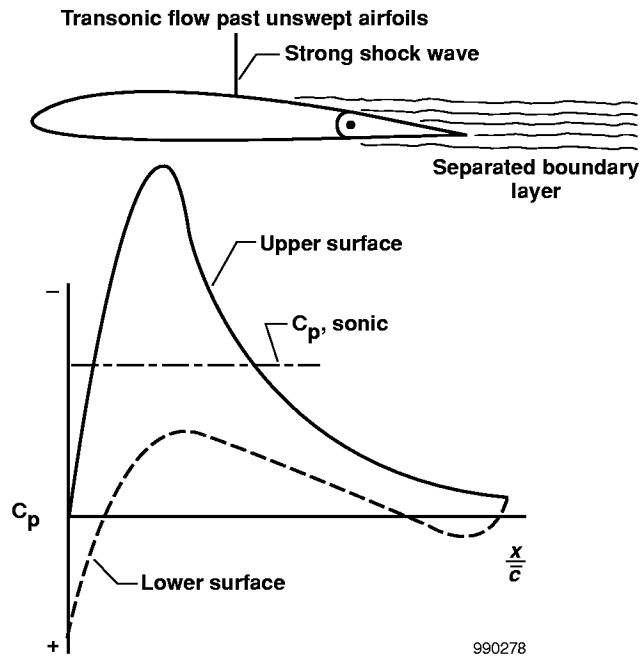


(c) Supercritical Mach number.

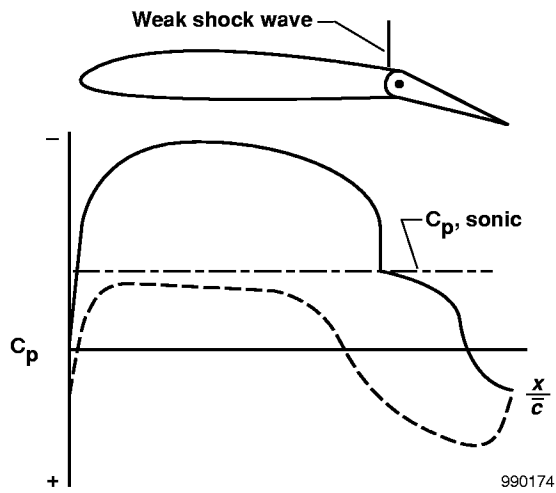


(d) Transonic Mach number.

Figure 8. Shock formation (schematic).²⁰



(a) Faired trailing edge ($\delta = 0$).



(b) Trailing-edge-down deflection.

Figure 9. Influence of trailing-edge deflection on profile pressure distribution and weak shock wave (schematic).

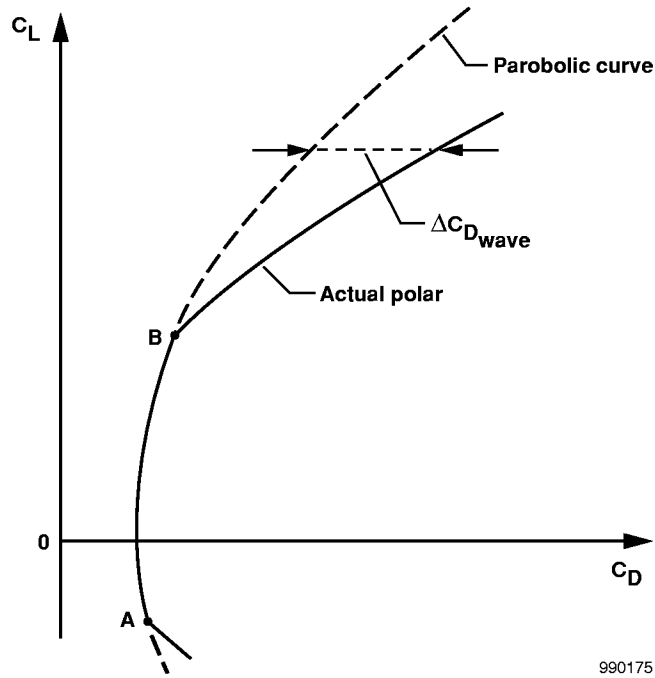


Figure 10. Polar of aircraft for transonic field (schematic).

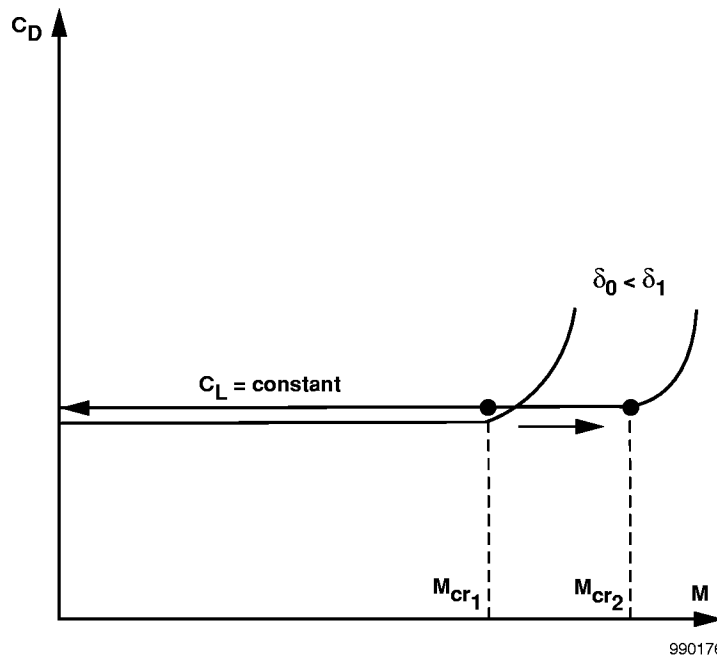


Figure 11. Drag coefficients as a function of Mach number and trailing-edge (flap) deflection (schematic).

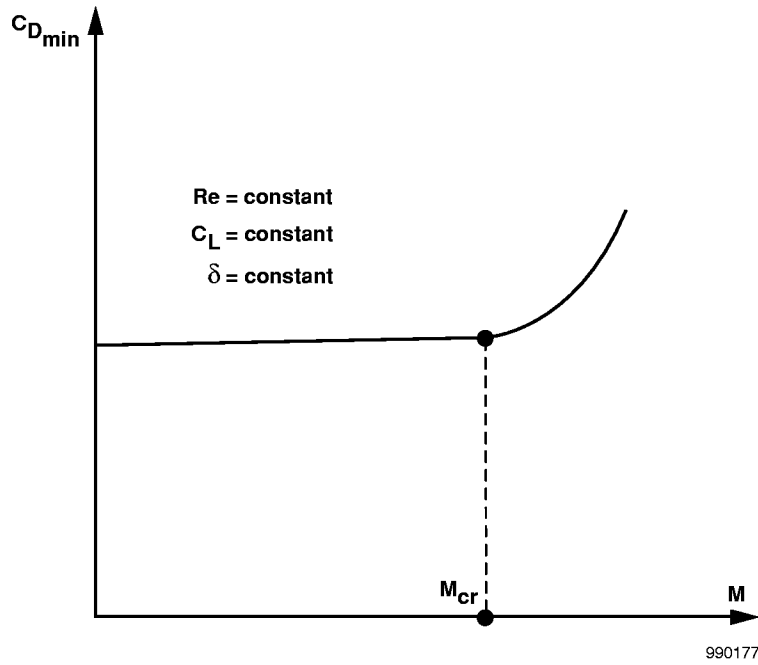


Figure 12. Minimum drag coefficient as a function of Mach number (schematic).

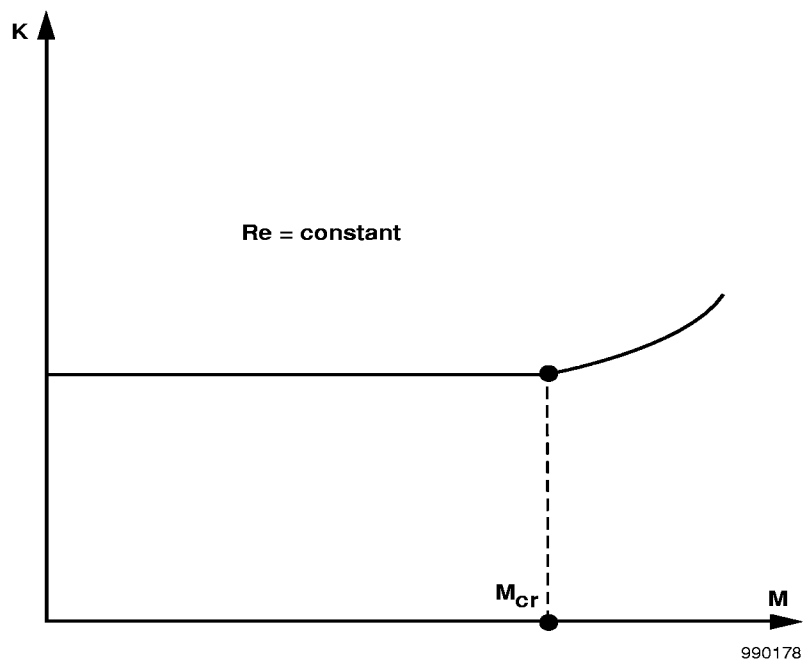


Figure 13. Efficiency factor K as a function of Mach number (schematic).

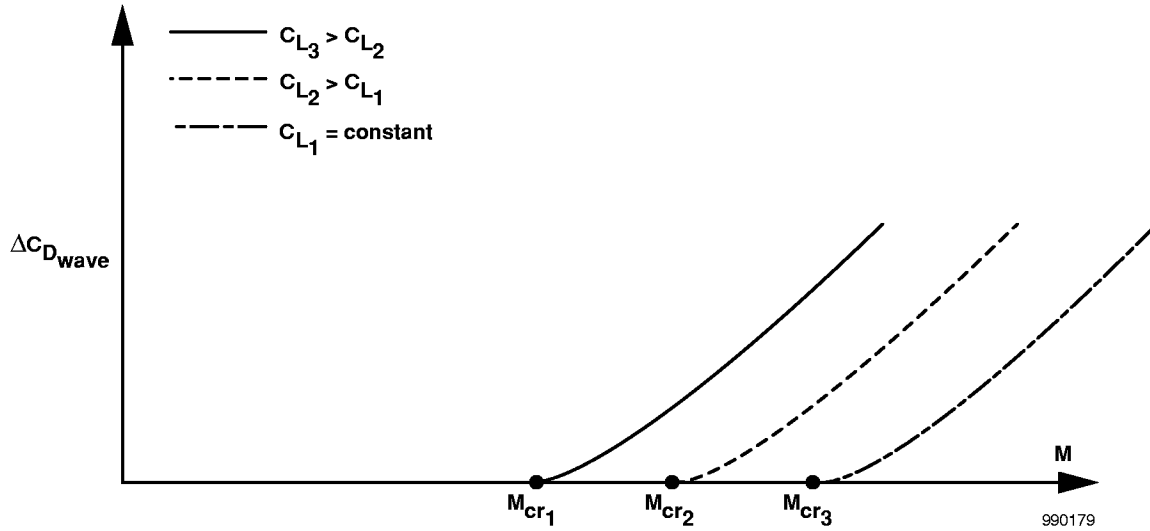


Figure 14. Wave drag coefficient as a function of Mach number and C_L (schematic).

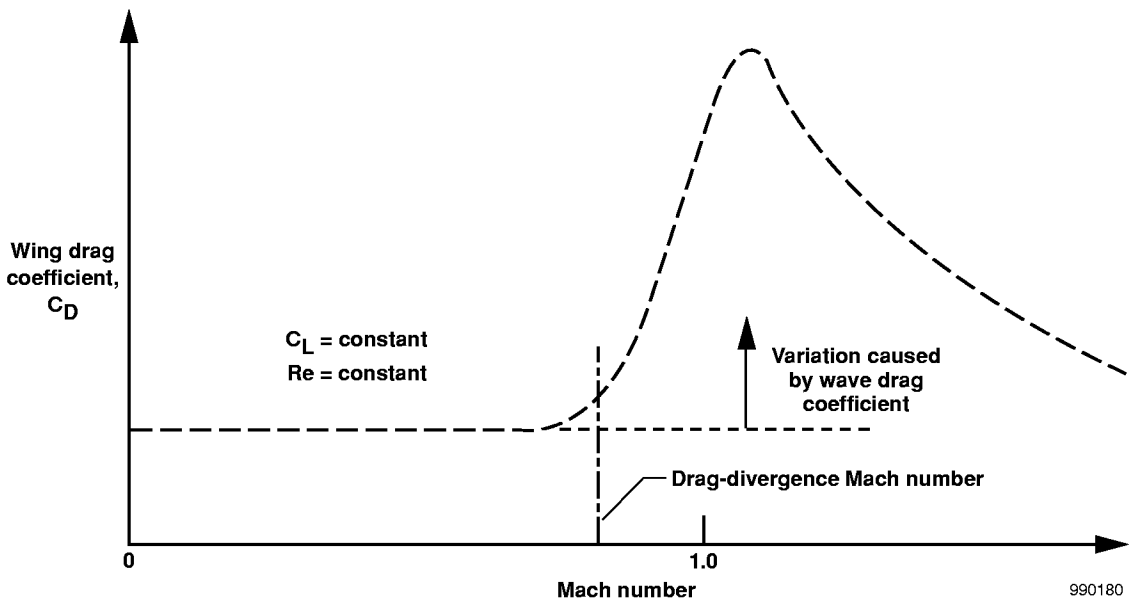
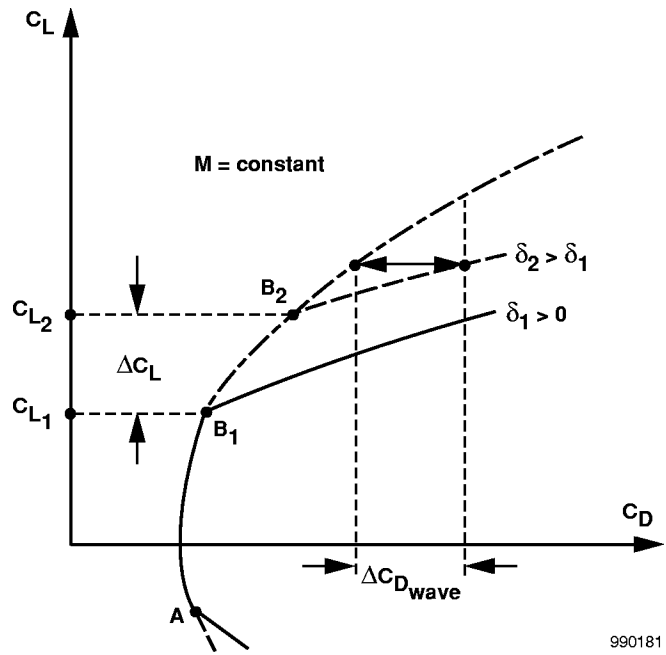
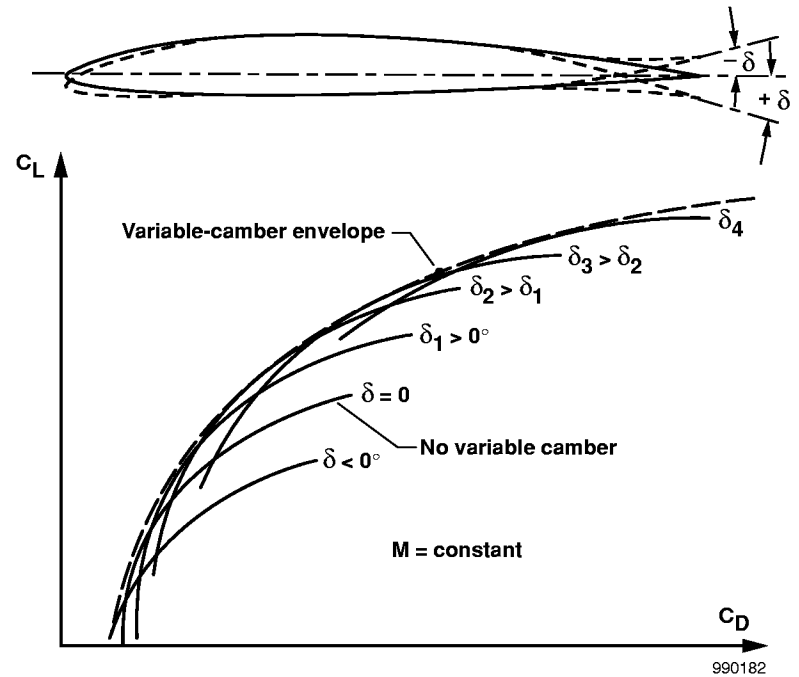


Figure 15. Variation of wing drag coefficient with Mach number (schematic).



990181

Figure 16. Polar of airplane as a function of the flap deflection (schematic).



990182

Figure 17. Variation of drag polar as a function of trailing-edge deflection (schematic).

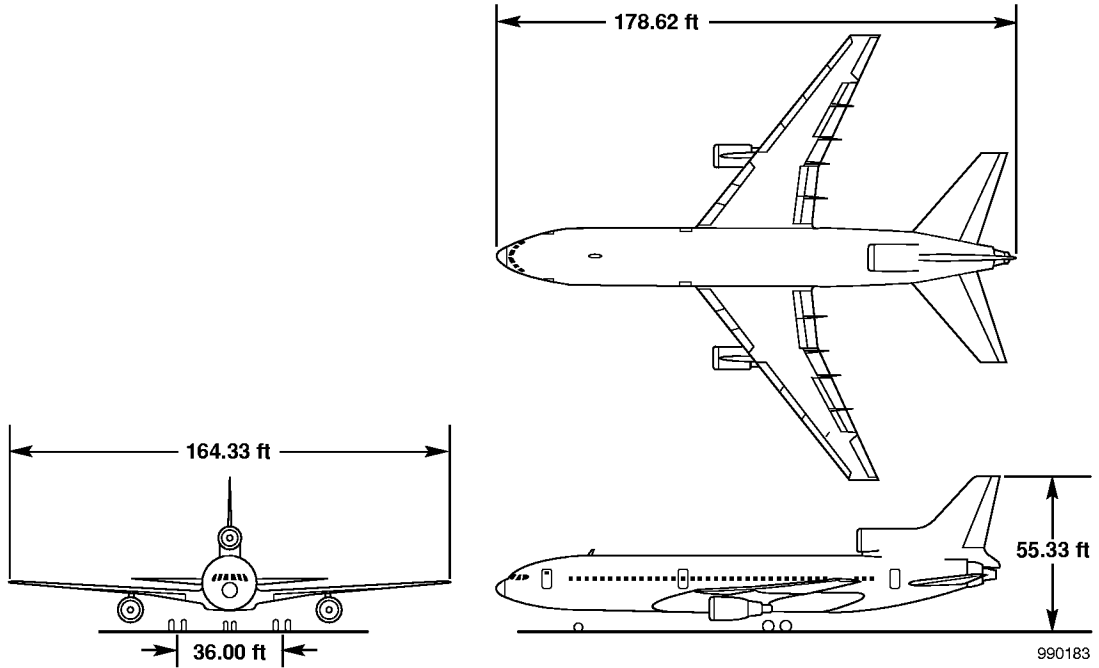


Figure 18. The L-1011 airplane.

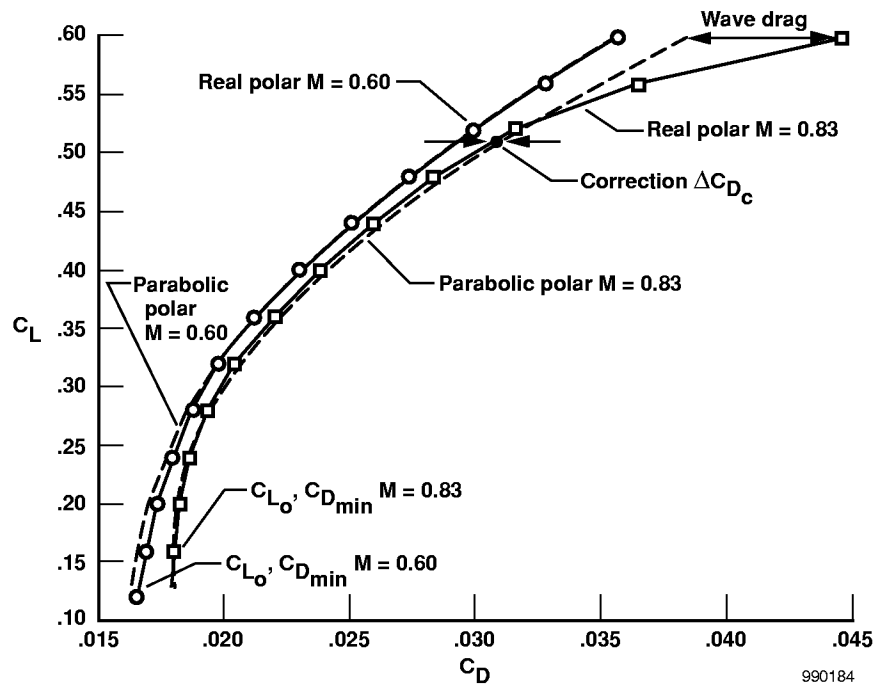


Figure 19. Real and parabolic polar of the L-1011 airplane for Mach 0.60 and Mach 0.83.

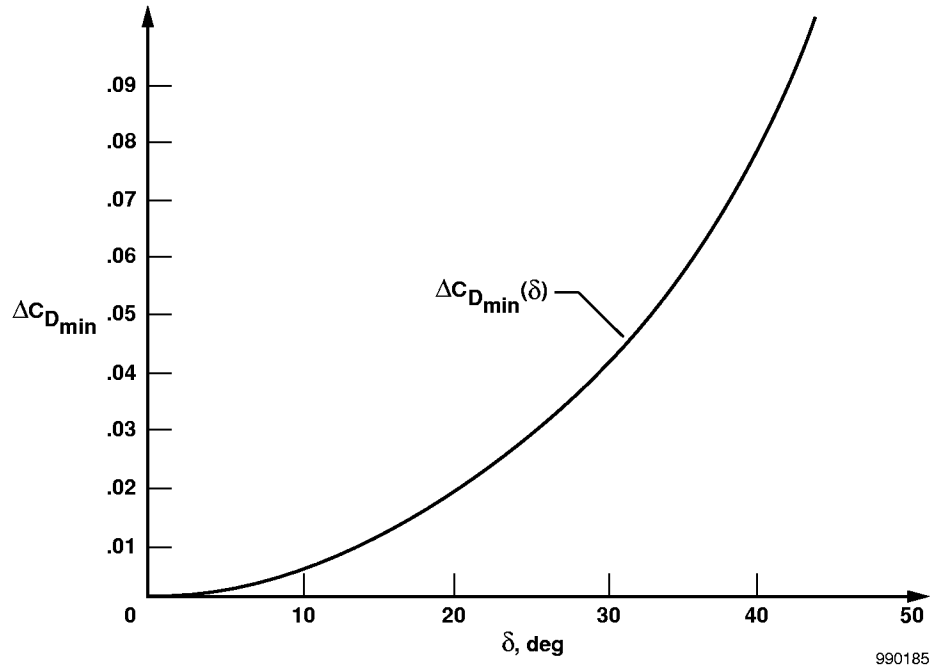
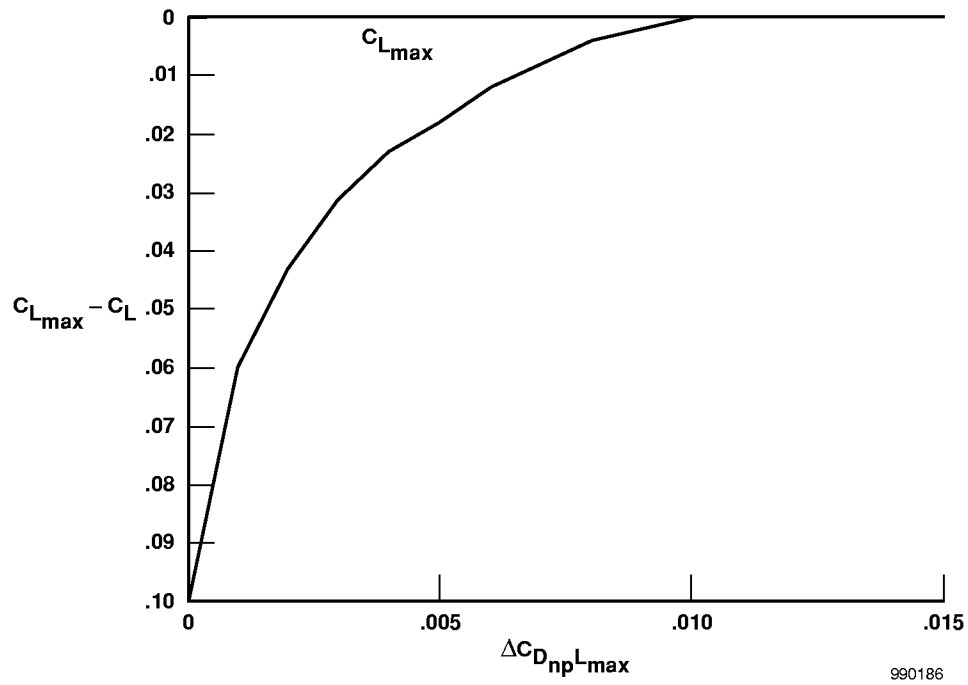
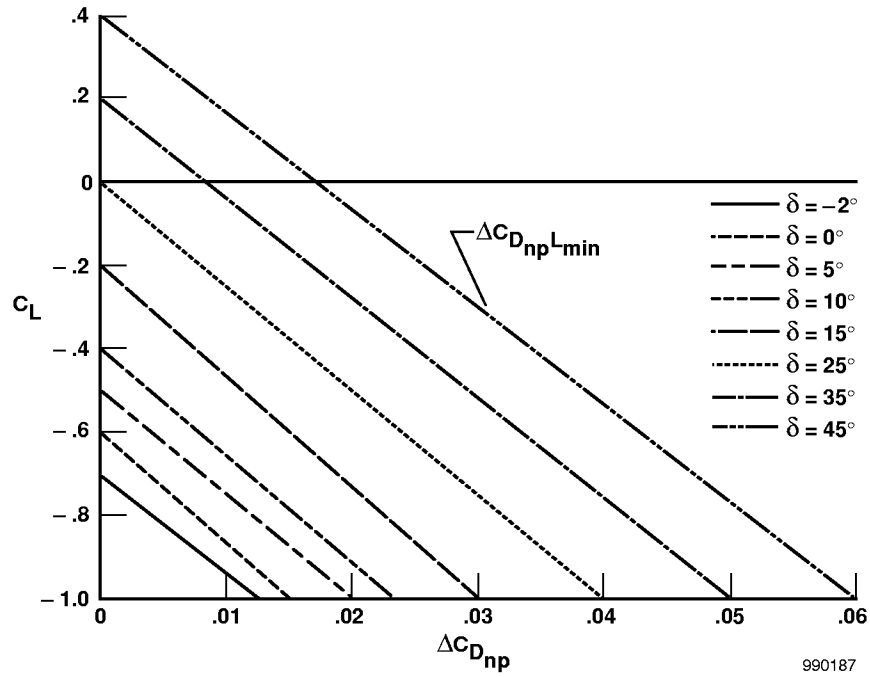


Figure 20. Decrement of minimum drag coefficient as a function of trailing-edge (flap) deflection.



(a) Decrement of drag coefficient ($C_{L_{max}} - C_L$).

Figure 21. Nonparabolic variation of drag coefficient.



(b) Decrement of drag coefficient as a function of trailing-edge (flap) deflection.

Figure 21. Concluded.

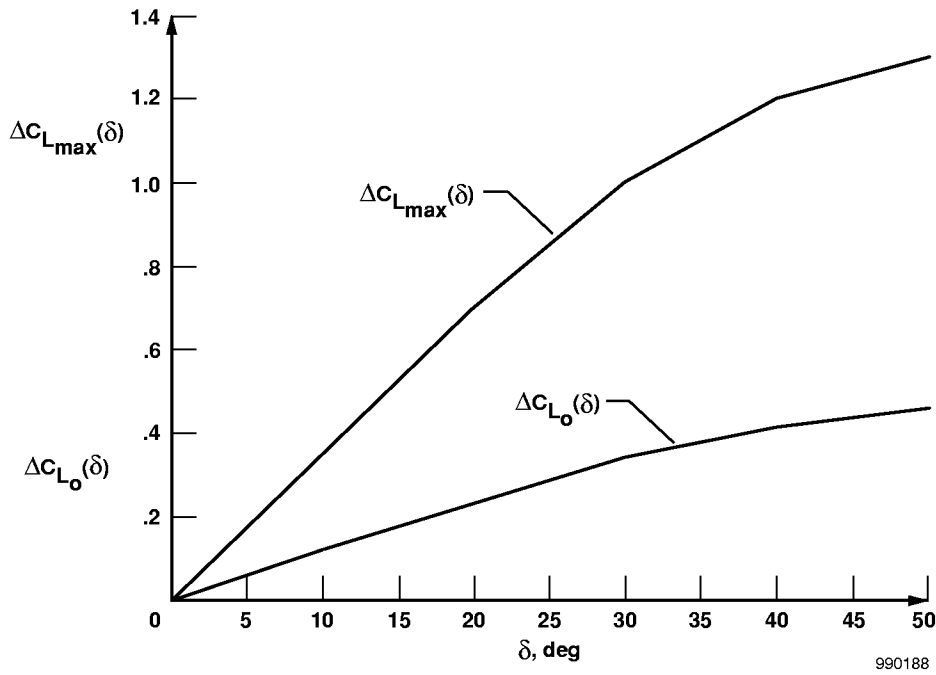


Figure 22. Decrement of the lift coefficient as a function of the trailing-edge (flap) deflection.

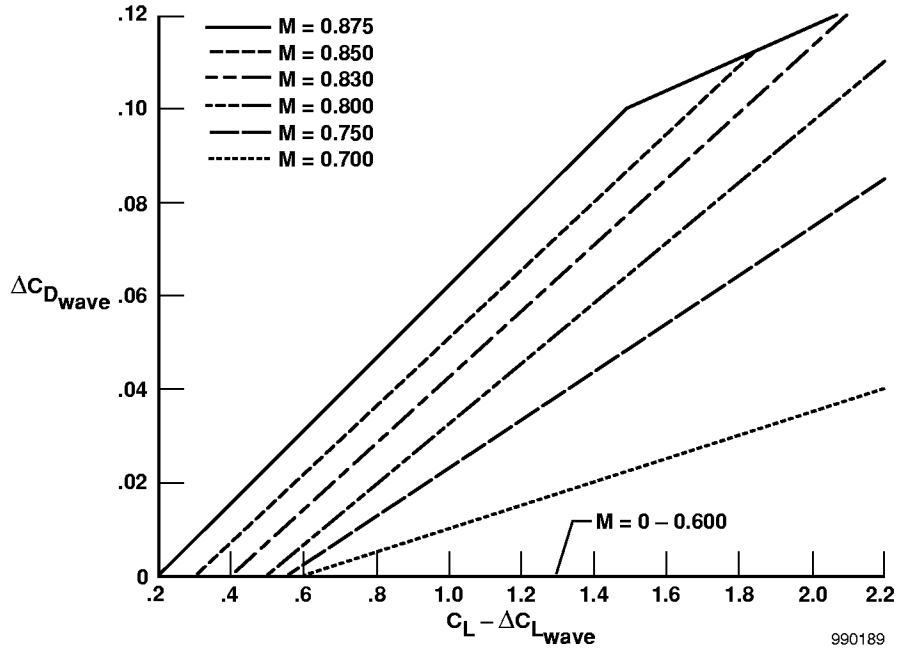


Figure 23. Increment of wave drag coefficient as a function of the lift coefficient and Mach number.

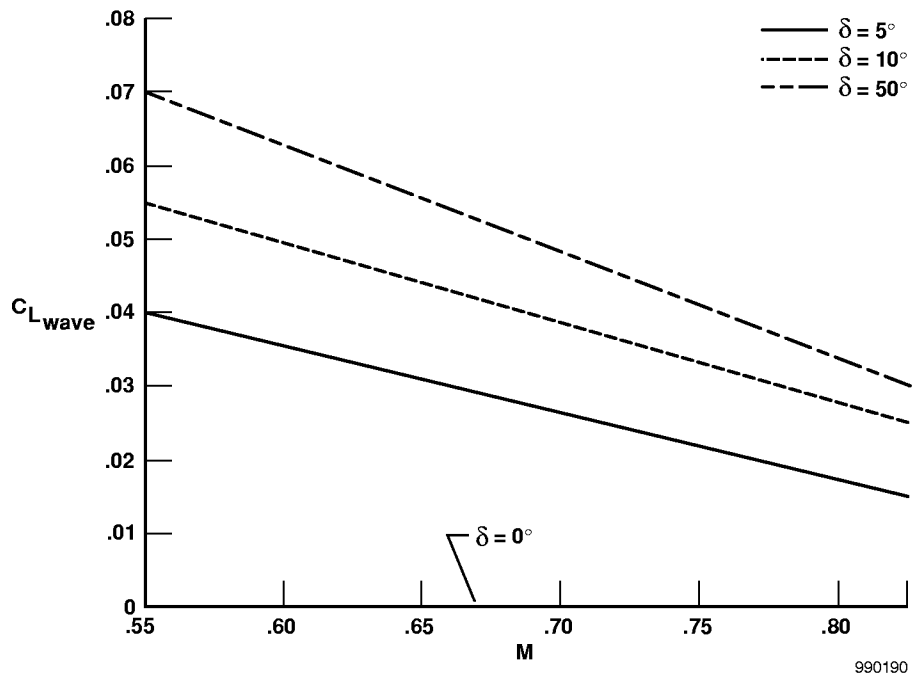


Figure 24. Increment of the critical lift coefficient as a function of Mach number and trailing-edge (flap) deflection.

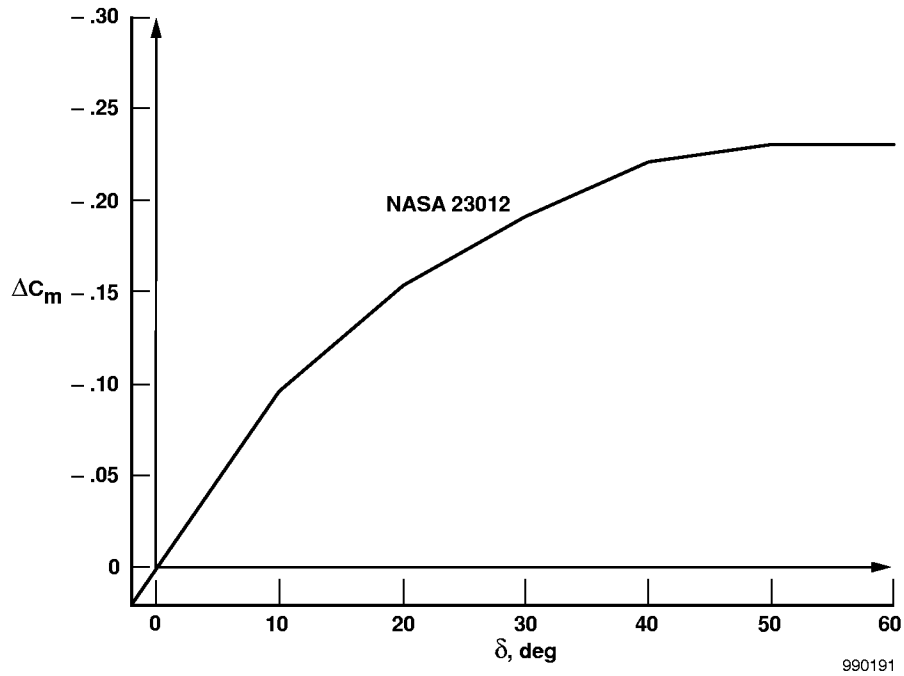


Figure 25. Incremental pitching moment from variable camber (flat-plate flap) from typical airfoil (NASA 23012).

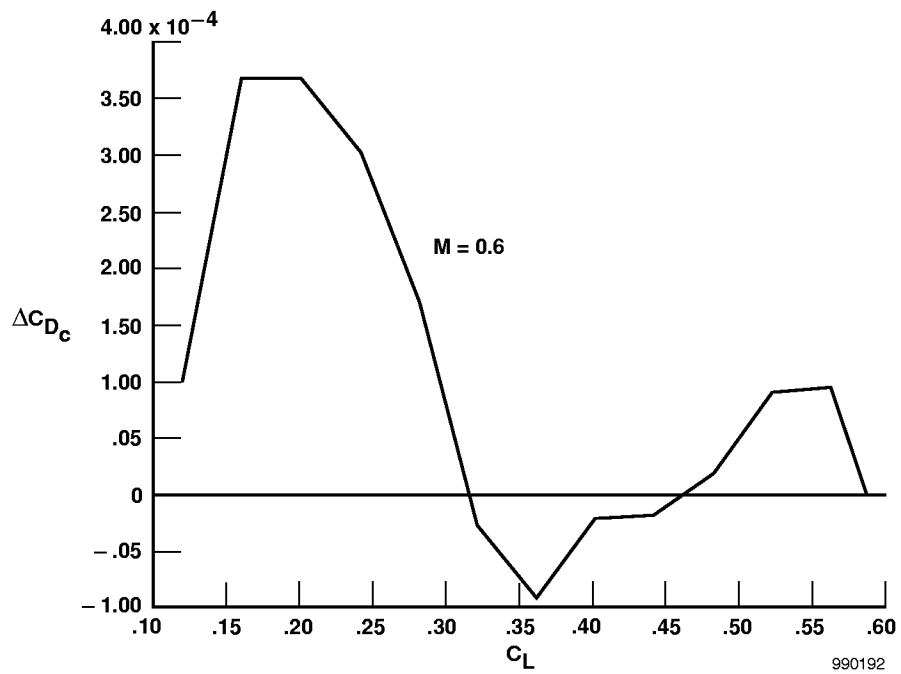


Figure 26. Correction on real polar for Mach 0.60.

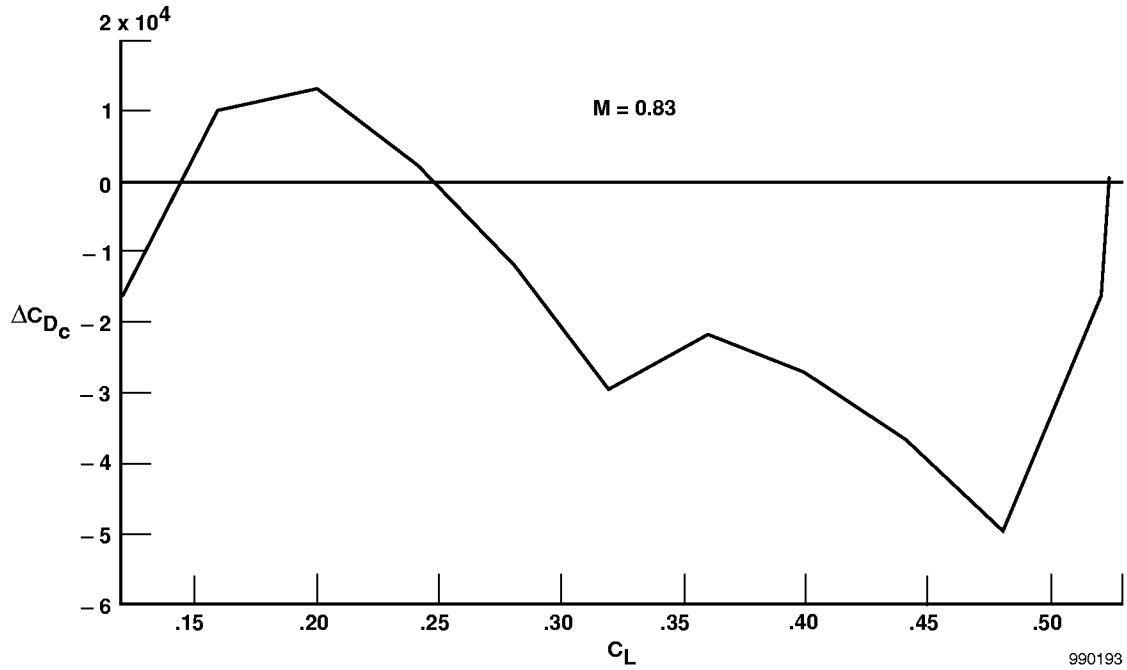


Figure 27. Correction on real polar for Mach 0.83.

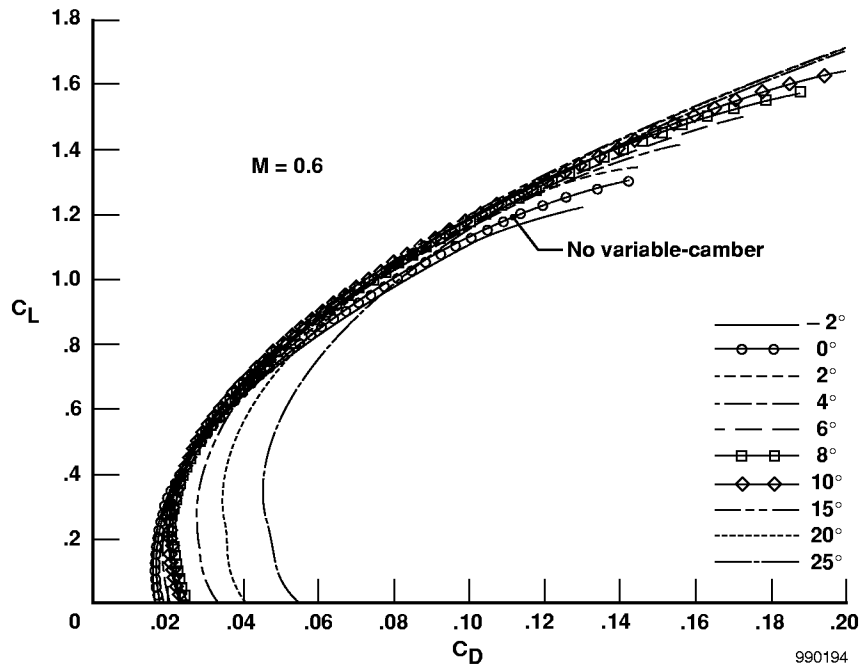


Figure 28. A family of polars of the L-1011 aircraft with variable camber for different deflection of trailing-edge angles at Mach 0.60.

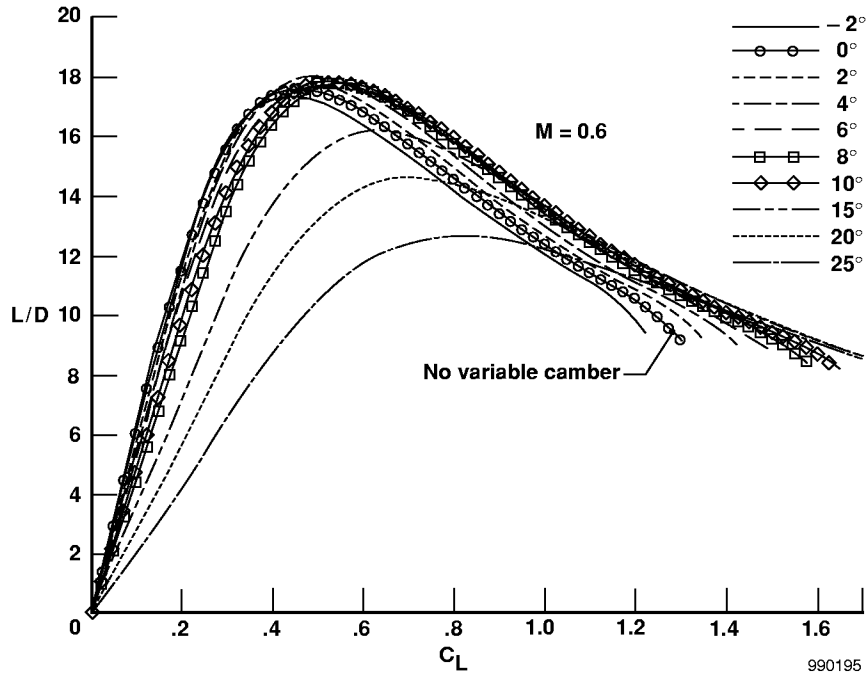


Figure 29. Relation of L/D variation with C_L for a range of trailing-edge deflections.

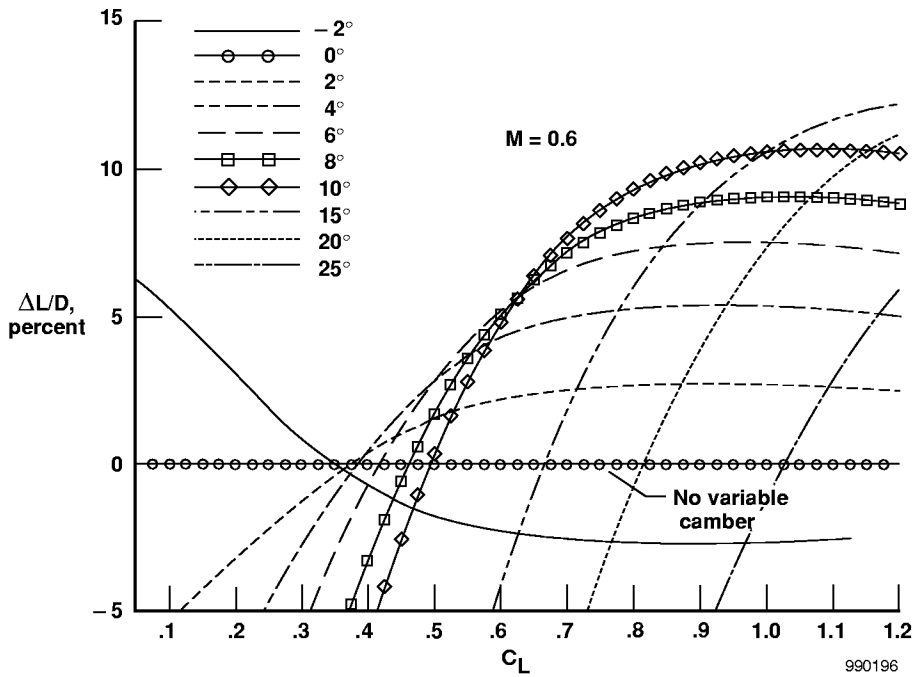


Figure 30. Incremental $\Delta L/D$ performance benefit variation with trailing-edge deflections.

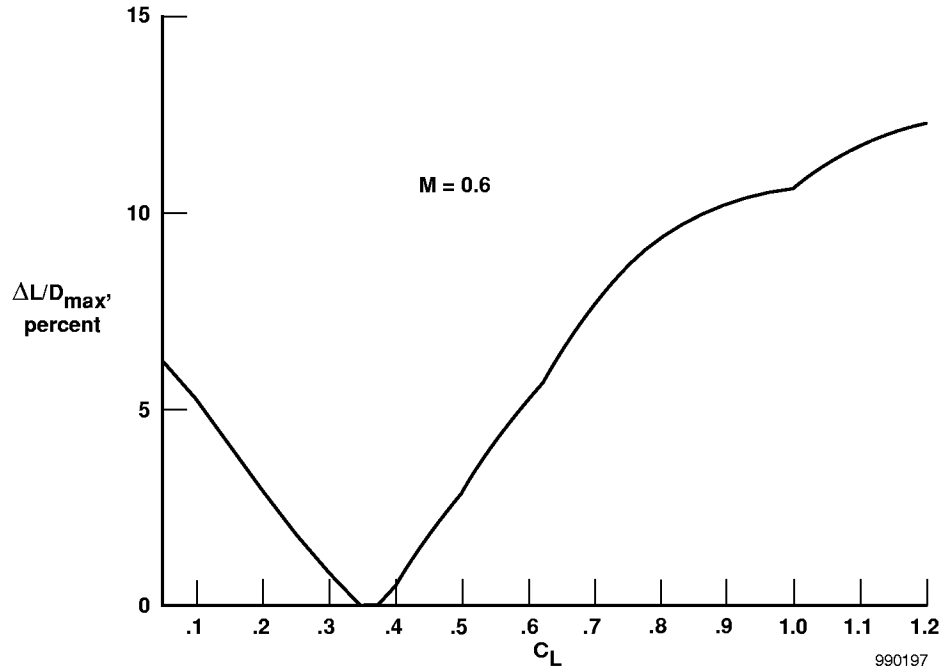


Figure 31. Maximum increment of $\Delta L/D$ benefit at Mach 0.60.

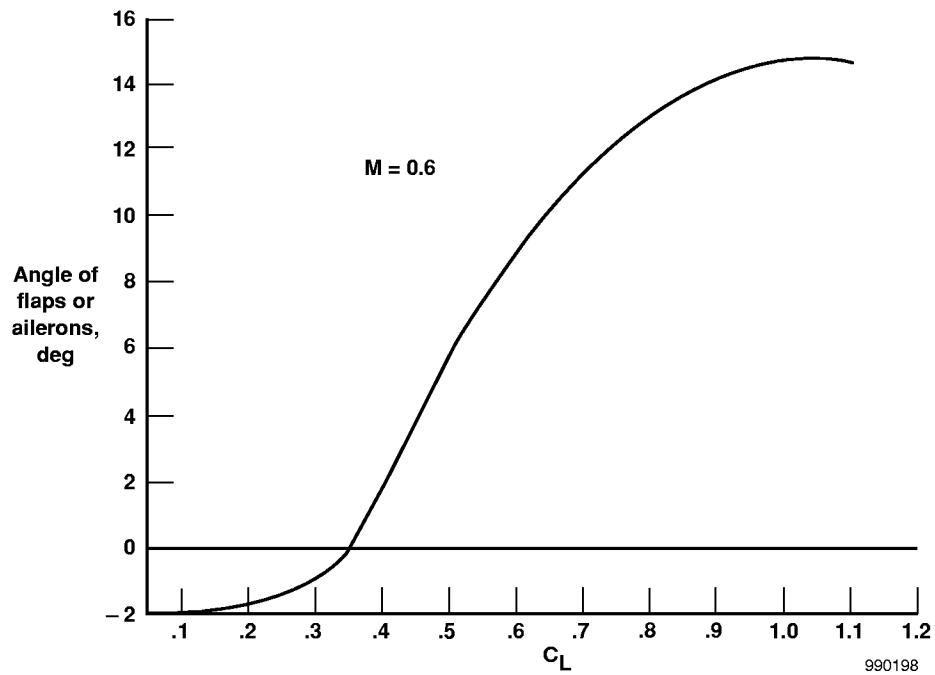


Figure 32. Optimal angle of trailing edge at Mach 0.60 (outer locus of fig. 30).

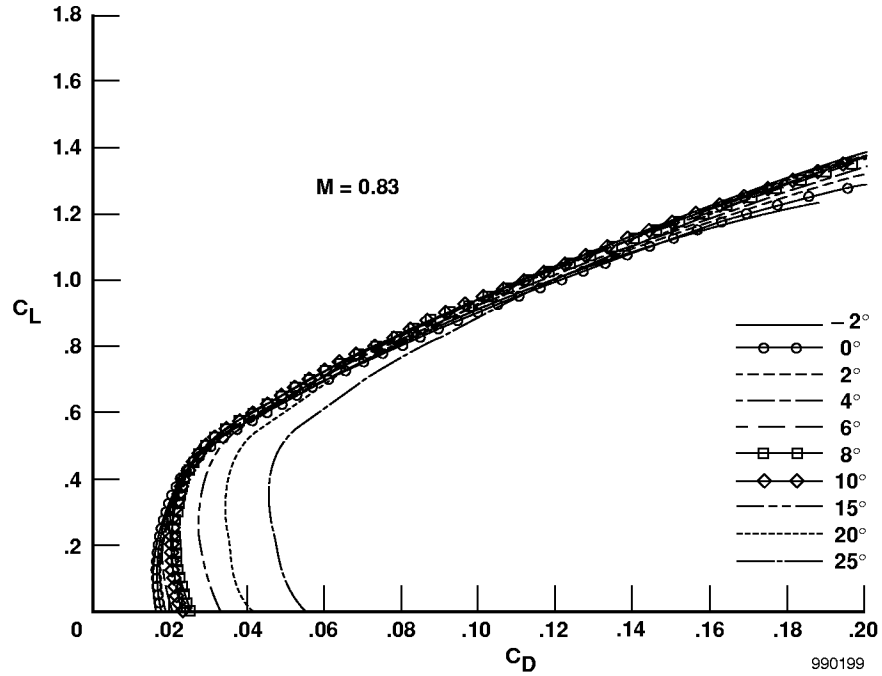


Figure 33. A family of polars for different deflections of trailing-edge angles at Mach 0.83.

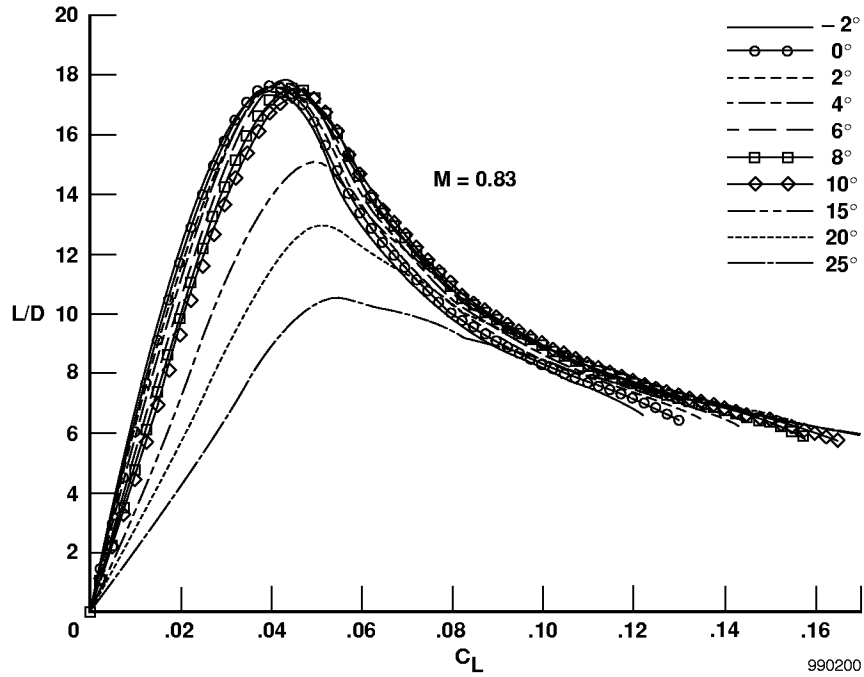


Figure 34. Relation $E = C_L / C_D$ for different flap deflections at Mach 0.83.

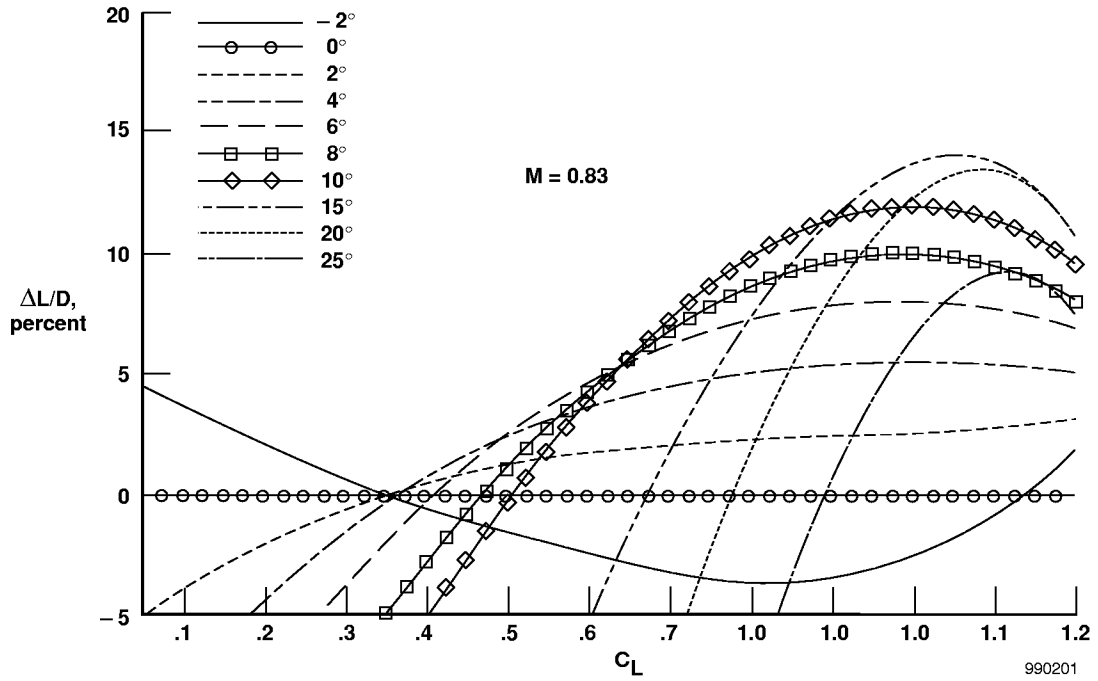


Figure 35. Increment ΔE (percent) for different flap deflection at Mach 0.83.

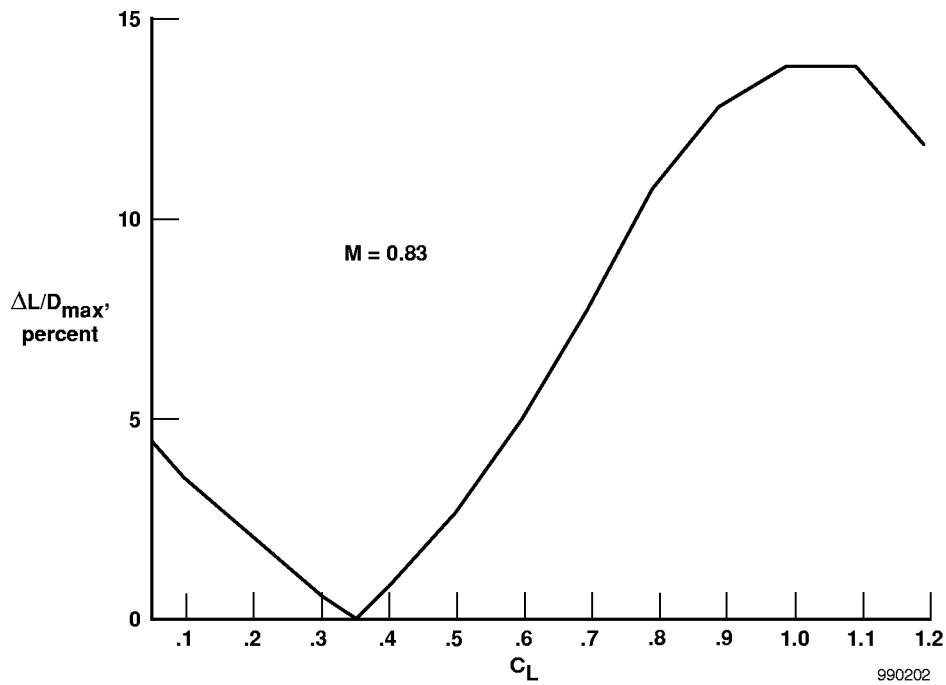


Figure 36. Maximum increment $\Delta L/D$ benefit at Mach 0.83.

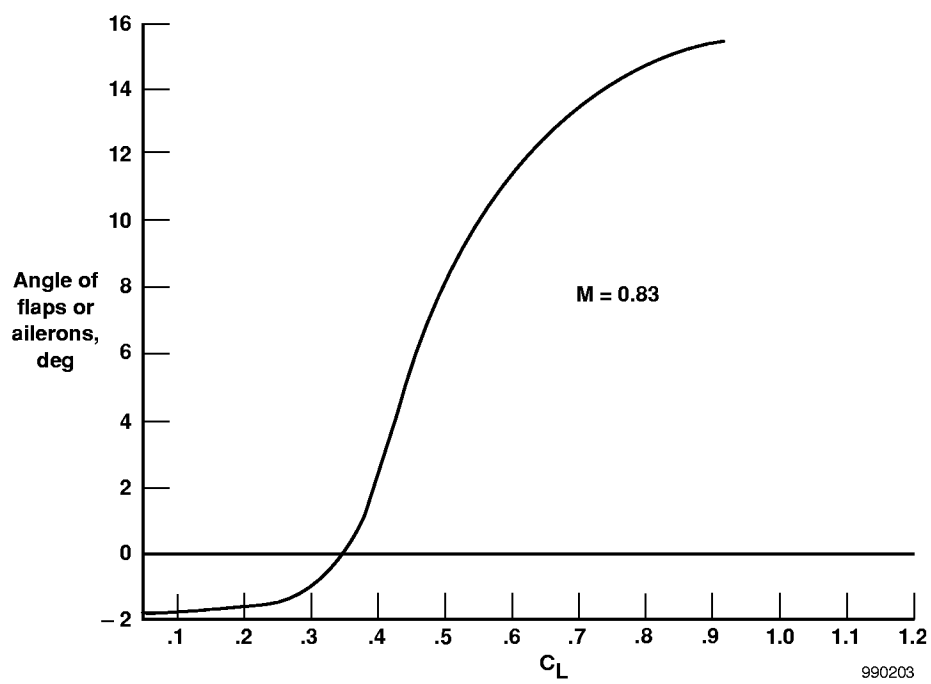


Figure 37. Optimal angle of trailing edge.

REPORT DOCUMENTATION PAGE

Form Approved
OMB No. 0704-0188

Public reporting burden for this collection of information is estimated to average 1 hour per response, including the time for reviewing instructions, searching existing data sources, gathering and maintaining the data needed, and completing and reviewing the collection of information. Send comments regarding this burden estimate or any other aspect of this collection of information, including suggestions for reducing this burden, to Washington Headquarters Services, Directorate for Information Operations and Reports, 1215 Jefferson Davis Highway, Suite 1204, Arlington, VA 22202-4302, and to the Office of Management and Budget, Paperwork Reduction Project (0704-0188), Washington, DC 20503.

| | | | | |
|--|--|---|---|--|
| 1. AGENCY USE ONLY (Leave blank) | | 2. REPORT DATE October 1999 | 3. REPORT TYPE AND DATES COVERED Technical Memorandum | |
| 4. TITLE AND SUBTITLE Estimated Benefits of Variable-Geometry Wing Camber Control for Transport Aircraft. | | | 5. FUNDING NUMBERS WU 522 16 14 00 39 00 L10 | |
| 6. AUTHOR(S) Alexander Bolonkin and Glenn B. Gilyard | | | | |
| 7. PERFORMING ORGANIZATION NAME(S) AND ADDRESS(ES) NASA Dryden Flight Research Center P.O. Box 273 Edwards, California 93523-0273 | | | 8. PERFORMING ORGANIZATION REPORT NUMBER H-2368 | |
| 9. SPONSORING/MONITORING AGENCY NAME(S) AND ADDRESS(ES) National Aeronautics and Space Administration Washington, DC 20546-0001 | | | 10. SPONSORING/MONITORING AGENCY REPORT NUMBER NASA/TM-1999-206586 | |
| 11. SUPPLEMENTARY NOTES Alexander Bolonkin, Senior Research Associate of the National Research Council, Washington D. C. and Glenn B. Gilyard, NASA Dryden Flight Research Center, Edwards, California. | | | | |
| 12a. DISTRIBUTION/AVAILABILITY STATEMENT Unclassified—Unlimited Subject Categories 02-01, 02-03, 03-01 | | | 12b. DISTRIBUTION CODE | |
| 13. ABSTRACT (Maximum 200 words) Analytical benefits of variable-camber capability on subsonic transport aircraft are explored. Using aerodynamic performance models, including drag as a function of deflection angle for control surfaces of interest, optimal performance benefits of variable camber are calculated. Results demonstrate that if all wing trailing-edge surfaces are available for optimization, drag can be significantly reduced at most points within the flight envelope. The optimization approach developed and illustrated for flight uses variable camber for optimization of aerodynamic efficiency (maximizing the lift-to-drag ratio). Most transport aircraft have significant latent capability in this area. Wing camber control that can affect performance optimization for transport aircraft includes symmetric use of ailerons and flaps. In this paper, drag characteristics for aileron and flap deflections are computed based on analytical and wind-tunnel data. All calculations based on predictions for the subject aircraft and the optimal surface deflection are obtained by simple interpolation for given conditions. An algorithm is also presented for computation of optimal surface deflection for given conditions. Benefits of variable camber for a transport configuration using a simple trailing-edge control surface system can approach more than 10 percent, especially for nonstandard flight conditions. In the cruise regime, the benefit is 1–3 percent. | | | | |
| 14. SUBJECT TERMS Adaptive control, Aircraft performance, Cambered wings, Commercial aircraft, Lift-to-Drag ratio, Optimization, Variable-camber wing. | | | 15. NUMBER OF PAGES 50 | |
| | | | 16. PRICE CODE A03 | |
| 17. SECURITY CLASSIFICATION OF REPORT Unclassified | 18. SECURITY CLASSIFICATION OF THIS PAGE Unclassified | 19. SECURITY CLASSIFICATION OF ABSTRACT Unclassified | 20. LIMITATION OF ABSTRACT Unlimited | |